

Cosmic Ray Streaming in Clusters of Galaxies

Joshua Wiener¹, S. Peng Oh¹, & Fulai Guo^{2 3}

¹*Department of Physics; University of California; Santa Barbara, CA 93106, USA.*

²*Department of Astronomy & Astrophysics, University of California, Santa Cruz, CA 95064, USA.*

³*ETH Zürich, Institute for Astronomy, Wolfgang-Pauli-Strasse 27, CH-8093, Zürich, Switzerland*

1 May 2018

ABSTRACT

The observed bimodality in radio luminosity in galaxy clusters is puzzling. We investigate the possibility that cosmic-ray (CR) streaming in the intra-cluster medium can ‘switch off’ hadronically induced radio and gamma-ray emission. For self-confined CRs, this depends on the source of MHD wave damping: if only non-linear Landau damping operates, then CRs stream on the slow Alfvénic timescale, but if turbulent wave damping operates, super-Alfvénic streaming is possible. As turbulence increases, it promotes outward streaming more than it enables inward turbulent advection. Curiously, the CR flux is *independent* of ∇f (as long as it is non-zero) and depends only on plasma parameters; this enables radio halos with flat inferred CR profiles to turn off. We perform 1D time-dependent calculations of a radio mini-halo (Perseus) and giant radio halo (Coma) and find that both diminish in radio luminosity by an order of magnitude in several hundred Myr, given plausible estimates for the magnetic field in the outskirts of the cluster. Due to the energy dependence of CR streaming, spectral curvature develops, and radio halos turn off more slowly at low frequencies – properties consistent with observations. Similarly, CR streaming rapidly turns off gamma-ray emission at the high-energies probed by Cherenkov telescopes, but not at the low energies probed by *Fermi*. CR mediated wave-heating of the ICM is unaffected, as it is dominated by \sim GeV CRs which stream Alfvénically.

Key words: radiation mechanisms: non-thermal, turbulence, galaxies: clusters: general, radio continuum: general, X-rays: general

1 INTRODUCTION

Cosmic rays (CRs) in the intra-cluster medium (ICM) can arise from structure formation shocks (Miniati et al. 2001; Pfrommer 2008), turbulent reacceleration of existing non-thermal particles (Brunetti & Lazarian 2007), galactic winds and supernovae (Völk, Aharonian & Breitschwerdt 1996), and radio galaxy jets (Enßlin et al. 1997; Ensslin et al. 1998; McNamara & Nulsen 2007). They are visible in clusters in radio emission, and gamma-ray emission (via hadronic interactions). However, unlike in our interstellar medium (ISM), CRs in the ICM are energetically subdominant; for instance, current upper limits on CR-induced gamma-ray emission in Perseus suggest CRs are $\lesssim 1 - 2\%$ of the thermal energy density (Aleksić et al. 2012). Why then are CRs in clusters of astrophysical significance? Firstly, unlike in the ISM, cosmic ray protons (CRp) with $E \lesssim 10^7$ GeV remain confined and have lifetimes of order a Hubble time (Völk, Aharonian & Breitschwerdt 1996; Berezhinsky, Blasi & Ptuskin 1997); they therefore encode archaeological information about the cluster assembly history as well as AGN and supernova activity. Secondly, the ICM provides stringent tests of plasma

physics in a regime very different from the ISM. CRs in clusters represent an opportunity to study the unknown efficiency of shock acceleration (Blandford & Eichler 1987) in a low Mach number $\mathcal{M} \sim 1 - 5$ and high plasma beta $\beta \sim 100$ regime. Transient radio phenomena can also teach us about magnetic field amplification at shocks. Thirdly, even a low level of CRs could have interesting astrophysical implications. These range from pressure support (thus affecting the use of clusters for cosmology) to heating which suppresses cooling flows (Guo & Oh 2008) or energizes filaments (Ferland et al. 2008, 2009), and distributing metals and heat via buoyancy-induced turbulent convection (Chandran & Rasera 2007; Sharma et al. 2009).

One drawback of cosmological simulations of CRs in clusters is that they generally do not include CR transport processes; the CRs are assumed to be frozen into the gas, and advected with it. In practice, CRs can move relative to the gas by streaming along magnetic field lines down a CR gradient, as well as diffusing across field lines by scattering off plasma waves. As CRs stream, their momentum anisotropy excites plasma waves, which in turn scatter the CRs, isotropizing the CR distribution in the frame of the

waves. This generally limits streaming speeds to the speed of the waves, which is the Alfvén speed v_A . In our ISM, rapid pitch-angle scattering due to the CR streaming instability¹ (Lerche 1967; Kulsrud & Pearce 1969; Wentzel 1969; Skilling 1971) can explain the observed spatial isotropy of CRs, as well as the escape time of CRs from the Galaxy (Schlickeiser 2002; Kulsrud 2005). Applying the same CR self-confinement scenario to the ICM, the low implied drift speed of CRs $v_D \sim v_A \sim 100 \text{ km s}^{-1}$, seems to justify neglect of cosmic ray transport. Early calculations of CRs in isolated clusters (Boehringer & Morfill 1988; Loewenstein, Zweibel & Begelman 1991) which considered CR diffusion at a level comparable to ISM values found it to be negligible as a transport process. They argued that if CRs were injected at the cluster center by an AGN, they would quickly dominate pressure support at a level inconsistent with observations. Guo & Oh (2008) resolved this in their calculations of CR heating by allowing CRs to be transported by rising buoyant bubbles, as seen in high resolution Chandra images, which are subsequently shredded by Kelvin-Helmholtz and Rayleigh-Taylor instabilities to disperse the CRs.

However, this assumption of slow CR streaming and diffusion may not be fully justified. The plasma waves which scatter the CRs are also subject to a variety of damping mechanisms. If damping is stronger in the ICM than in the ISM, then pitch-angle scattering of the CRs off the attenuated waves will be reduced, and the CRs retain some momentum anisotropy in the frame of the waves. They can therefore stream faster than the waves, and will no longer be limited by the Alfvén speed. In principle, if the waves are very strongly damped, the CRs could stream up at speeds up to $\sim c$. While the possibility of super-Alfvénic or even free streaming was appreciated early on (Kulsrud & Pearce 1969; Kulsrud & Cesarsky 1971; Skilling 1971), generally $v_D \sim v_A$ and diffusion coefficients appropriate for the ISM have been uncritically applied to the ICM environment. In an influential recent paper, Enßlin et al. (2011) noted the interesting possibility of super-Alfvénic streaming in the ICM, adopted the sound speed c_s as a characteristic streaming speed, and were the first to discuss the wide-ranging observational consequences.

A particularly interesting possibility they focused on was whether the interplay between advection and streaming could be responsible for the observed bimodality seen in radio halo luminosity. Giant radio halos are generally only seen in disturbed clusters which show signs of merger activity. This bimodality has been a stumbling block for hadronic models (e.g., Pfrommer & Enßlin (2004)). These models track the long-lived CR protons (CRp) formed during structure formation shocks, and find that the secondary electrons formed when the CRps undergo hadronic interactions are sufficient to explain radio halo observations. Transience or correlation with turbulence is generally not expected in such

¹ In principle, CRs can also scatter off MHD turbulence, though this is thought to be weak due to the increasing anisotropy at small scales, with power concentrated in modes with wavevectors transverse to the B-field, while CRs efficiently scatter off the parallel component (Chandran 2000; Yan & Lazarian 2002). Fast magnetosonic modes could potentially scatter CRs more efficiently (Brunetti & Lazarian 2007), but a treatment of this is beyond the scope of this paper.

models. As a result, radio halos are often attributed to the re-energization of seed electrons by Fermi II acceleration when the ICM turbulence becomes transonic during mergers (Brunetti et al. 2001; Brunetti & Lazarian 2007). As the turbulence dies away, the CR electrons (CRE) cool via synchrotron and inverse Compton emission on a relatively short ($\sim 10^8$ yr) timescale. However, the origin of the seed electrons is uncertain; low energy electrons will rapidly Coulomb cool in the dense cluster center. Enßlin et al. (2011) suggested instead that transonic turbulence advects CRs from the plentiful reservoir on the cluster outskirts. Hadronic interactions of the inwardly advected CRp with the dense central ICM can then produce CRE². Once turbulence dies down, subsequent outward CR streaming switches off the radio halo. This rapid outward streaming also explains why radio halos turn off in the original hadronic scenario, which is otherwise difficult to understand. For these explanations to work, the CR streaming timescale must be relatively short, or $v_D \gg v_A$. Enßlin et al. (2011) adopted $v_D \sim c_s$ and examined its implications, but only justified this assumption qualitatively.

This paper aims to critically examine the possibility that super-Alfvénic streaming could play a crucial role in CR transport in the ICM, by building more quantitative models to clarify its plausibility and importance. It has three main goals: (i) a quantitative calculation of CR streaming speeds in quasi-linear theory and its dependence on plasma parameters, when a variety of wave damping mechanisms are at play. In particular, we consider the effects of non-linear Landau damping and turbulent damping. We also give expressions for parallel diffusivities and CR heating rates in this regime. Of particular interest is the countervailing effects of turbulence: it affects CR transport both by turbulent advection of CRs from the cluster outskirts, as well as damping of CR generated waves, which enables faster outward streaming. We assess their relative importance. (ii) A reevaluation of CR heating due to central injection by an AGN (Guo & Oh 2008), taking these streaming effects into account. (iii) A 1D simulation of radio halo turnoff due to CR streaming, to establish if the required dimming by at least an order of magnitude can take place within a reasonable timescale. We also calculate how the gamma-ray luminosity evolves with time. A non-linear, time-dependent calculation is needed since the streaming speed itself depends on CR energy density. In their analytic calculations, Enßlin et al. (2011) consider a steady-state profile where inward turbulent advection and outward CR streaming are in rough balance. This scenario seems somewhat unlikely; it seems more probable that at a given point in time, either inward advection or outward streaming dominates. To calculate radio halo turnoff, we consider the latter. These calculations also enable us to compute a fundamental prediction of this model: spectral steepening and frequency-dependent dimming which arise from energy-dependent streaming speeds. We compare these with observations.

The outline of this paper is as follows. In §2, we calculate in quasi-linear theory cosmic-ray streaming speeds when different wave damping mechanisms are dominant, and de-

² Alternatively, low energy relic CRE advected from the cluster outskirts could provide seeds for turbulent reacceleration.

rive expressions for the resulting parallel diffusivity, as well as turbulent diffusion rates. In §3, we describe the equations we solve numerically with ZEUS, focusing in particular on the CR transport equation. We describe our initial conditions for the cosmic ray profile, which are tuned to match radio halo observations for the Perseus and Coma clusters. We also present a test case of CR heating by a central AGN. In §4, we present the results of simulations of radio halo turnoff due to CR streaming. In §5, we show how aspects of these results can be understood analytically. Finally, we conclude in §6.

2 COSMIC RAY STREAMING: QUASI-LINEAR THEORY

In this section, we derive the basic equations we use, in particular the streaming speeds and diffusion coefficients which are used in the cosmic-ray transport equation. Our treatment is by design semi-quantitative rather than fully rigorous.

2.1 Cosmic Ray Streaming

2.1.1 Resonant Scattering and Wave Growth

Consider a cosmic ray proton with Lorentz factor γ propagating along a magnetic field line of strength B_0 with cyclotron frequency $\Omega_0 = eB_0/(m_p c)$, gyroradius $r_L = \gamma c/\Omega_0$, and pitch angle cosine μ . Since $v_A \ll c$, Alfvén waves are perceived by the CR as a spatially varying but time-stationary B-field. An Alfvén wave is resonant with this cosmic ray if it has a wave vector \mathbf{k} whose component parallel to the magnetic field k_{\parallel} equals the parallel projection of the gyroradius, i.e. if the resonance condition

$$k_{\parallel} = \frac{1}{\mu r_L} \quad (1)$$

is satisfied. This resonance is a requirement both for the wave to scatter the CR and for the CR to excite the wave. This condition can be easily understood: if the magnetic field changes on a length scale much longer than the projected gyroradius, the CR will simply follow the field line adiabatically, with no change in pitch angle. If the field varies on much smaller scales, the CR will see a rapidly oscillating Lorentz force during its orbit and remain unaffected, essentially only seeing the background field. At resonance, the CR sees a constant field due to the wave, and hence a steady force. The k_{\parallel} portion of the wave is the relevant one, since it has a transverse magnetic field δB_{\perp} which can exert a Lorentz force on the v_{\parallel} component of a streaming cosmic-ray.

If the distribution of cosmic rays in the frame of the Alfvén waves is completely isotropic, then the effect of a cosmic ray traveling along the magnetic field line in one direction is cancelled by an equivalent cosmic ray traveling in the opposite direction, and there is no wave growth. However, Kulsrud & Pearce (1969) showed that even a slight anisotropy in the cosmic rays—which naturally arises in the presence of sources and sinks—will cause unstable growth in the waves, caused by momentum transfer from the CRs to the waves in the course of pitch-angle scattering. The result-

ing wave growth rate is (Kulsrud & Pearce 1969):

$$\Gamma_{\text{CR}}(k_{\parallel}) \sim \Omega_0 \frac{n_{\text{CR}}(> \gamma)}{n_i} \left(\frac{v_D}{v_A} - 1 \right) \quad (2)$$

In the above, $n_{\text{CR}}(> \gamma)$ is the number density of cosmic ray protons with energies large enough to be resonant with the Alfvén wave for some pitch angle μ , namely $r_L > 1/k_{\parallel}$ (though since the CR spectrum falls off rapidly with energy, generally $k_{\parallel} \sim 1/r_L$), n_i is the ion density in the plasma, and v_D and v_A are the cosmic ray streaming and Alfvén speeds respectively. This expression is derived from balancing CR momentum loss with wave momentum gain, but we can understand its main features qualitatively. The rate of wave growth scales with that for momentum loss for a single CR, $\dot{p} \propto p\Omega_{\text{rel}} = (\gamma mc^2)(\Omega_0/\gamma) \propto \Omega_0$, i.e. the non-relativistic, rather than the relativistic gyro-frequency. This has to be multiplied by the fraction of ions which can drive wave growth, $n_{\text{CR}}(> \gamma)/n_i$ (non-resonant ions simply provide inertia, slowing down wave growth), and the anisotropy which seeds the wave growth $(v_D/v_A - 1)$.

The streaming instability causes the waves to grow until pitch-angle scattering renders the CR distribution isotropic in the frame of the waves, i.e. $v_D \sim v_A$. If we assume $(v_D/v_A - 1) \sim \mathcal{O}(1)$, we can estimate the growth time of the waves. If we assume that the energy density in CRs is $\sim 10\%$ of the thermal energy density, $\epsilon_{\text{CR}} \sim 0.1\epsilon_{\text{therm}}$, then $n_{\text{CR}}(E_{\text{CR}}) \sim 0.1n_i \langle E_i \rangle$ where $\langle E_{\text{CR}} \rangle \sim \text{GeV}$ (as is true for most reasonable power-law momentum distributions—e.g., see Fig. 1 of Enblin et al. (2007)), and $\langle E_i \rangle \sim \text{keV}$ are the typical energies of CRs and thermal ions respectively, and so $n_{\text{CR}}/n_i \sim 10^{-7}$. A similar ratio holds in the coronal regions of our Galaxy. For $\sim \mu\text{G}$ fields, $\Omega_0 = eB/mc \sim 10^{-2} \text{ s}^{-1}$, implying from equation (2) a wave growth time of $\Gamma_{\text{CR}}^{-1} \sim 30 \text{ yr}$, i.e. extremely short.

The above arguments suggest that self-confinement of cosmic-rays is very efficient, and should always reduce the streaming velocities $v_D \sim v_A$. The general success of the self-confinement picture for our Galaxy means that this has been uncritically assumed in other environments such as the ICM, and/or CR diffusion coefficients scaled to the measured Galactic values. In fact, v_D , and the associated diffusion coefficient D_{θ} depend on the amplitude of the wave field $\delta B/B$, which can be calculated by assuming equilibrium between growth and damping. If damping processes are sufficiently strong, then $\delta B/B$ will be insufficient to efficiently confine the CRs, and super-Alfvénic streaming is possible. We now examine this possibility.

2.1.2 Non-linear Landau Damping

Parallel propagating MHD waves do not suffer any linear damping. However, they can undergo non-linear Landau damping when two waves A & B of slightly different frequency interact to form a beat wave. This beat wave can resonantly interact with thermal particles with parallel velocity identical to the wave's phase speed, $v_{\parallel} = (\omega_A - \omega_B)/(k_A - k_B)$ (for parallel propagating waves, $v_{\parallel} = v_A$). Particles moving more slowly than the beat wave will extract energy from the wave (thus damping it), while particles moving faster than the wave will add energy to it. For a Maxwellian plasma,

typically $(\partial f/\partial v)_{v_{\parallel}=v_A} < 0$, and damping dominates.³ The high frequency wave gives up energy to a combination of the low frequency wave and resonant particles.

To aid in physical insight, we present a simplified derivation of streaming speeds to be expected if non-linear Landau damping dominates, before employing the formulae from more detailed derivations (Lee & Völk 1973; Kulsrud 1978; Felice & Kulsrud 2001). The damping rate in a high- β plasma is (Kulsrud 2005):

$$\Gamma_{\text{NL}} \approx \frac{1}{2} \sqrt{\frac{\pi}{2}} \left(\frac{v_i}{v_A} \right) \left(\frac{\delta B}{B} \right)^2 \omega \approx 0.3 \frac{\Omega}{\mu} \frac{v_i}{c} \left(\frac{\delta B}{B} \right)^2 \quad (3)$$

How can we qualitatively understand the first relation? The wave frequency $\omega = k_{\parallel} v_A$ sets the fundamental frequency, while interactions involving the beat wave arise to second-order in perturbed field strength $(\delta B/B)^2$. Since the resonant condition $v_{\parallel} = \mu v_i = v_A$ implies that thermal particles with $\mu = v_A/v_i$ are resonant, it is clear that the damping rate should depend on this ratio. However, the exact dependence only emerges from a detailed calculation—either by calculating the slope $(\partial f/\partial v)_{v_{\parallel}=v_A}$, or from the plasma dispersion relation (Foote & Kulsrud 1979). Note that since $v_i/v_A = \beta^{1/2}/2$, we have $\Gamma_{\text{NL}} \propto \beta^{1/2}$. In the second relation, we use the dispersion relation $\omega = k_{\parallel} v_A$ and the resonance condition, equation (1).

In steady state, the Vlasov equation for CRs is (Kulsrud & Pearce 1969):

$$v_z \frac{\partial f}{\partial z} = \frac{\partial}{\partial \mu} \left[\frac{1 - \mu^2}{2} \nu(\mu) \frac{\partial f}{\partial \mu} \right] \quad (4)$$

where $B = B_z \hat{z}$, $\nu(\mu) \approx \Omega(\delta B/B)^2$ and $v_z = \mu c$. This expresses the condition that the net streaming along field lines is set by diffusion in pitch-angle. In the limit of strong scattering, we can expand $f = f_0 + f_1 + f_2 + \dots$ where $f_0(p, z, t)$ is isotropic and $f_1(p, z, t, \mu) \ll f_0$, $f_2 \ll f_1$. Let us also define $\mathcal{F} = f_1/f_0$ and the scale height $L_z(p, z) = f_0/(\partial f/\partial z)$. Integrating both sides of equation (4) with respect to μ and dividing by f_0 , we obtain:

$$\frac{\partial \mathcal{F}}{\partial \mu} = -\frac{c}{\nu L_z}. \quad (5)$$

If we set

$$\mathcal{F} = 1 + \frac{3(v_D - v_A)}{c} \mu \quad (6)$$

so that $\langle \mu c \mathcal{F}(\mu) \rangle = (v_D - v_A)$ (i.e., the leading order anisotropy in the distribution function yields the net drift relative to the frame of the waves), this yields:

$$(v_D - v_A) \approx \frac{r_L}{3L_z} \left(\frac{\delta B}{B} \right)^{-2} c \approx \frac{\lambda}{3L_z} c \quad (7)$$

where $\lambda \sim r_L(\delta B/B)^{-2}$ is the mean free path. In steady state, the wave growth rate (equation (2)) equals the wave damping rate (equation (3)). Together with equation (7), this gives us two equations which we can solve for two unknowns, v_D and $(\delta B/B)^2$. The result is:

$$\left(\frac{\delta B}{B} \right)^2 = \left(\frac{c}{v_A} \frac{c}{v_i} \frac{r_0}{3L_z} \frac{n_{\text{CR}}(>\gamma)}{n_i} \gamma^2 \right)^{1/2} \quad (8)$$

where $f_0 \propto p^{-n}$ (note that our result differs from Felice & Kulsrud (2001), who explicitly specialize to $\gamma \sim 5$ for the ISM from the outset). If we scale to numbers characteristic of the ICM, we obtain:

$$\left(\frac{\delta B}{B} \right)^2 = 1.6 \times 10^{-6} \frac{(n_{-10}^{\text{CR}})^{1/2} \gamma_{100}^{(5-n)/2} 10^{4.6-n}}{(n_{-3}^i)^{1/4} B_{\mu\text{G}} T_{4\text{keV}}^{1/4} L_{z,100}^{1/2}} \quad (9)$$

where $T_{4\text{keV}} = (T/4\text{keV})$, $B_{\mu\text{G}} = (B/1\mu\text{G})$, $L_{z,100} = (L_z/100\text{kpc})$, $n_{-3}^i = (n_i/10^{-3}\text{cm}^{-3})$, $n_{-10}^{\text{CR}} = n^{\text{CR}}(\gamma > 1)/10^{-10}\text{cm}^{-3}$, $\gamma_{100} = \gamma/100$, and we have scaled to $n = 4.6$. Note that $n^{\text{CR}}(>\gamma) = 10^{-10} \gamma^{-1.6} \text{cm}^{-3}$ roughly corresponds to a CR energy density in equipartition with a $\sim \mu\text{G}$ B-field. The fact that $(\delta B/B)^2 \ll 1$ self-consistently implies that quasi-linear theory is applicable. If we insert this into equation (7), we obtain for the drift speed:

$$v_D = v_A \left(1 + 0.9 \frac{(n_{-3}^i)^{3/4} T_{4\text{keV}}^{1/4} 10^{n-4.6}}{B_{\mu\text{G}} L_{z,100}^{1/2} (n_{-10}^{\text{CR}})^{1/2}} \gamma_{100}^{(n-3)/2} \right) \quad (10)$$

Several points should be noted. For these parameters, streaming speeds do not significantly exceed the Alfvén speed for the ~ 100 GeV cosmic-ray protons which in turn produce the 10 GeV CR electrons which in turn produce $\sim \text{GHz}$ radio emission. For Alfvén speeds of $v_A \approx 70 \text{ km s}^{-1} B_{\mu\text{G}} n_{i,-3}^{-1/2}$, this implies radio halo turnoff times of $t \sim 1.4 \text{ Gyr } L_{100} B_{\mu\text{G}}^{-1} n_{i,-3}^{1/2}$, which may seem too long. However, note that L_z, n^{CR} will be time-dependent functions during the streaming process, so it is necessary to check how streaming evolves in a time-dependent calculation. Our results should be contrasted with those of Enßlin et al. (2011), who describe similar estimates based on Felice & Kulsrud (2001), but do not give explicit expressions. Unlike them, we find $v_D \ll c_s$ for plasma parameters corresponding to observed clusters; nothing in the problem singles out the sound speed as a reference speed. Note that all the parameters in equation (10) are observationally constrained, so order of magnitude departures are unlikely. Also note that even though $\Gamma_{\text{NL}} \propto \beta^{1/2}$, there is no explicit β dependence in v_D .

2.1.3 Turbulent Damping

Another source of wave damping comes from the highly anisotropic nature of MHD turbulence (Farmer & Goldreich 2004; Yan & Lazarian 2002). We adopt the Goldreich & Sridhar (1995) theory (hereafter ‘GS’) for strong, incompressible MHD turbulence; an excellent summary can be found in Lithwick & Goldreich (2001). Turbulence in clusters is generally incompressible since it is significantly subsonic except at the cluster periphery. The strong turbulence regime where GS theory is applicable sets in at wavenumbers $k \lesssim k_o M_A^{-2}$ (e.g., see Nazarenko & Schekochihin (2011)); since $M_A \gtrsim 1$ in clusters, the theory is clearly applicable, particularly at the small scales relevant for CR scattering. GS theory has support both from numerical simulations (Cho & Vishniac 2000; Maron & Goldreich 2001) and solar wind measurements (Horbury, Forman & Oughton 2008; Podesta 2009;

³ In a high β plasma, $(\partial f/\partial v)_{v_{\parallel}=v_A}$ is relatively flat for electrons, while still steep for ions; hence, ions dominate the damping rate (Miller 1991).

Wicks et al. 2010; Chen et al. 2011). It is anisotropic, with:

$$v_{\lambda_{\perp}} \sim v_A \left(\frac{\lambda_{\perp}}{L_{\text{MHD}}} \right)^{1/3} \sim (\epsilon \lambda_{\perp})^{1/3} \quad (11)$$

$$\frac{\Lambda_{\parallel}(\lambda_{\perp})}{\lambda_{\perp}} \sim \left(\frac{L_{\text{MHD}}}{\lambda_{\perp}} \right)^{1/3} \quad (12)$$

where λ_{\perp} is the length scale transverse to the local mean magnetic field, $v_{\lambda_{\perp}}$ is the rms velocity fluctuation across λ_{\perp} , $\Lambda_{\parallel}(\lambda_{\perp})$ is the length scale parallel to the local mean magnetic field across which the velocity fluctuation is $v_{\lambda_{\perp}}$, L_{MHD} is the length scale at which turbulence is excited with velocity perturbations comparable to the Alfvén speed v_A (i.e., with $M_A \sim 1$), and $\epsilon \sim v_{\lambda_{\perp}}^3 / \lambda_{\perp} \sim v_A^3 / L_{\text{MHD}}$ is the (constant) energy cascade rate per unit mass. Note that L_{MHD} is *defined* to be the scale at which $M_A = 1$; if turbulence is already sub-Alfvénic at the outer scale, then it should be considered an extrapolation. Equation (11) describes a standard Kolmogorov cascade in the transverse direction. Equation (12) indicates that an eddy becomes increasingly elongated along the magnetic field, $\Lambda_{\parallel} \gg \lambda_{\perp}$ as the cascade proceeds deep into the inertial range $\lambda_{\perp} \ll L_{\text{MHD}}$. It can be derived from the assumption of “critical balance”, which states that characteristic linear and non-linear interaction times are approximately equal at all scales (e.g., see Nazarenko & Schekochihin (2011)). Thus, the cascade proceeds primarily in the transverse direction, and most of the power is concentrated in modes with transverse wave vectors. Intuitively, we can understand this from the fact that in MHD turbulence, non-linear interactions arise from collisions of oppositely directed Alfvén wave packets travelling along field lines. A wave packet is distorted when it follows field lines perturbed by its collision partner; it cascades when the field lines along which it is propagating have spread by a distance comparable to λ_{\perp} . Since the magnetic and velocity fluctuations associated with Alfvén waves are transverse to the local mean field, the cascade proceeds primarily in the transverse direction.

Turbulence therefore suppresses the waves responsible for self-confinement of cosmic rays, since they cascade to smaller scales before they have an opportunity to scatter CRs. In particular, the small scale transverse components injected by the cascade mean that the CR no longer experiences a time-steady force in its orbit; instead it sees an oscillating force which leads to inefficient scattering. For these same reasons, MHD turbulence scatters CRs inefficiently (Chandran 2000; Yan & Lazarian 2002). The damping rate of a wave is simply the eddy turnover rate (Farmer & Goldreich 2004):

$$\Gamma_{\text{turb}} \sim \frac{v_{\lambda_{\perp}}}{\lambda_{\perp}} \sim \frac{\epsilon^{1/3}}{\lambda_{\perp}^{2/3}} \quad (13)$$

where we use equation (11). Growth rates are highest, and damping rates lowest, for the most closely parallel-propagating waves, i.e. those with the largest λ_{\perp} . Even if a CR-generated wave starts out as parallel-propagating, the turbulent cascade injects transverse components which subsequently cascade. The amplitude of magnetic field fluctuations across a scale λ_{\perp} thus define a minimal aspect ratio⁴ $(k_{\perp}/k_{\parallel})_{\text{min}} \sim \delta B(\lambda_{\perp})/B \sim v_{\lambda_{\perp}}/v_A \sim (\lambda_{\perp}/L_{\text{MHD}})^{1/3}$

⁴ This should not be confused with the eddy aspect ratio

(using equation (11) in the last step). From the resonance condition $k_{\parallel}^{-1} \sim r_L$, the smallest possible perpendicular wavenumber is $k_{\perp,\text{min}} \sim \epsilon^{1/4} (r_L v_A)^{-3/4}$. Inserting the largest possible perpendicular wavelength $\lambda_{\perp} \sim k_{\perp,\text{min}}$ into equation (13), the minimal damping rate for a wave with $k_{\parallel} \sim r_L^{-1}$ is (Farmer & Goldreich 2004):

$$\Gamma_{\text{turb,min}} \sim \left(\frac{\epsilon}{r_L v_A} \right)^{1/2}. \quad (14)$$

If in steady state we balance the wave growth rate (equation (2)) with this damping rate, we obtain a streaming speed:

$$v_D = v_A \left(1 + 1.2 \frac{B_{\mu\text{G}}^{1/2} n_{i,-3}^{1/2}}{L_{\text{MHD},100}^{1/2} n_{\text{CR},-10}} \gamma_{100}^{n-3.5} 10^{2(n-4.6)} \right) \quad (15)$$

where $L_{\text{MHD},100} = L_{\text{MHD}}/100$ kpc. We also obtain $(\delta B/B) \sim 10^{-3}$. At first blush, non-linear Landau damping and turbulent damping both seem to give similarly slow streaming speeds. However, note that $v_D - v_A \propto (n_{\text{CR}}^{-1/2}, n_{\text{CR}}^{-1})$ for these two sources of damping respectively. This difference becomes crucial during non-linear evolution, enabling CRs in the turbulent damping case to stream much more effectively.

2.1.4 General Remarks on Cosmic-Ray Streaming

We have now derived streaming speeds for two different damping mechanisms, which depend both on CR energy ($v_D \propto \gamma^{0.8}, \gamma^{1.1}$ for non-linear Landau damping and turbulent damping respectively) and plasma parameters – most notably the CR number density. The streaming speed is thus a function of both position and time, and is best self-consistently solved in a time-dependent calculation, as we will soon tackle.⁵ Before we forge ahead and use these expressions, there are several potential complications worth discussing.

Our streaming speeds for the ICM are characteristically of order the Alfvén speed, although this can vary spatially and temporally as plasma parameters vary, particularly the CR number density. Enßlin et al. (2011) argue against the Alfvén speed as a characteristic CR propagation speed in a high β plasma, arguing that in the limit where the background magnetic field $B \rightarrow 0$, this would imply that $v_D \approx v_A \rightarrow 0$, rather than $v_D \rightarrow c$, as might be expected if there is no magnetic field to couple the CRs to the plasma. Instead, they advocate the sound speed c_S as a characteristic streaming speed. We have several remarks. The streaming speeds we have calculated via quasi-linear theory assumes $(\delta B/B) \ll 1$, and we have checked that this condition is self-consistently fulfilled in the ICM (typically, $(\delta B/B) \sim 10^{-4}$), an amplitude similar to that inferred for the coronal gas in our Galaxy. The hypothetical limit $B \rightarrow 0$ (which is not realized in the ICM) clearly violates this assumption, and requires a fully non-linear calculation. There,

$\Lambda_{\parallel}(\lambda_{\perp})/\lambda_{\perp} \gg 1$, whereas we have $(\lambda_{\parallel}/\lambda_{\perp})_{\text{min}} < 1$. Typical eddies in the MHD cascade vary mostly in the transverse direction, $k_{\perp} \gg k_{\parallel}$, whereas we seek waves injected by CRs with the least possible transverse variation, $k_{\perp} \ll k_{\parallel}$.

⁵ We have also assume $n(> \gamma)$ to be a fixed power-law, whereas it steepens with time due to energy dependent streaming.

we might expect that instabilities generated by a current of streaming CRs (e.g., Bell (1978)) would nonetheless generate a B-field which will confine the CRs. Nothing in our calculations singles out the sound speed as a reference velocity.

The resonance condition, equation (1), shows that CRs of larger pitch angle ($\mu \rightarrow 0$) interact with waves of progressively shorter wavelength. However, growth rates $\Gamma_{\text{CR}} \propto \mu$ (e.g., Kulsrud (2005)), while non-linear Landau damping $\Gamma_{\text{NL}} \propto 1/\mu$ (equation (3)), so there is relatively little energy in such short wavelength waves as $\mu \rightarrow 0$. On the face of it, this would imply that it is impossible for particles to scatter across the $\theta = 90^\circ$ point via resonant scattering to reverse direction, the well-known ‘90° problem’ (in fact, the affected region is small; quasi-linear interactions can effectively scatter CRs down to $\mu_c \sim 10^{-4}$. The gap is a little larger, $\sim v_i/c \sim 3 \times 10^{-3}$, in a high- β plasma when ion-cyclotron damping is effective (Holman, Ionson & Scott 1979)). The fact that CRs appear to be efficiently confined and isotropized in our Galaxy implies that Nature has found a way around it. The leading explanation appears to be mirror interactions from MHD waves created by the $\theta \sim 0^\circ$ CRs, which are able to trap the particles and turn them around (Felice & Kulsrud 2001). These mirror interactions can also be thought of as resonance broadening (Achterberg 1981; Yan & Lazarian 2008) of the long wavelength waves. Felice & Kulsrud (2001) conduct a detailed boundary layer calculation of the mirror interaction and find that it introduces a minor logarithmic correction (which we have ignored) to the standard calculation. We note that if there were indeed a 90° problem in the ICM, the resulting light-speed streaming speeds would imply flat CRp and CRe profiles, which is inconsistent at least with observations of radio mini-halos such as Perseus. It would also shut off radio halos extremely rapidly, regardless of how the relativistic electrons are produced.

The wave damping rate is the sum of all damping processes, and thus in principle one should always consider the contribution from both turbulent and non-linear Landau damping. In practice, we consider limiting regimes where one process dominates. Their ratio is:

$$\frac{\Gamma_{\text{turb}}}{\Gamma_{\text{NL}}} \approx 1. \frac{B_{\mu\text{G}}^{3/2} n_{i,-3}^{1/4} L_{z,100}^{1/2}}{L_{\text{MHD},100}^{1/2} T_{4\text{keV}}^{1/4} n_{\text{CR},-10}^{1/2}} \gamma_{100}^{n/2-2} \propto \left(\frac{1}{\nabla f} \right)^{1/2}. \quad (16)$$

Turbulent damping thus always dominates at late times as the CR profile falls ($n_{\text{CR}} \rightarrow 0$) and flattens ($L_z \rightarrow \infty$).

We have only considered CR self-confinement, and ignored other possible mechanisms for scattering CRs. As we have previously discussed, the anisotropic nature of Alfvénic MHD turbulence (which is mostly transverse on small scales comparable to the gyro-radius, in contrast to the parallel modes required to scatter CRs) make them inefficient scatterers of CRs (Chandran 2000; Yan & Lazarian 2004). While the distribution of slow magnetosonic waves follows that of Alfvén waves (Lithwick & Goldreich 2001), fast magnetosonic modes can potentially have an independent non-linear cascade which is isotropic and can efficiently scatter CRs (Schlickeiser 2002; Brunetti & Lazarian 2007). For now, we eschew this possibility, in favor of the well-established self-confinement picture, which is the generally accepted theory in our Galaxy. One failing of the self-

confinement picture in our Galaxy is that both non-linear Landau damping and turbulent damping appear to damp the waves too efficiently at high energies; the increase of streaming speeds with energy appear inconsistent with the low observed CR anisotropy for $E > 100$ GeV (Farmer & Goldreich 2004). Chandran (2000) has proposed that magnetic mirror interactions in dense molecular clouds could provide this further confinement, though the possibility remains that some aspects of the physics are still not well understood. A conservative reading of these possible complications would take our derived streaming speeds and diffusion coefficients as upper bounds; they could potentially be lower if scattering is more efficient.

2.2 Cosmic-Ray Transport

2.2.1 Cosmic-Ray Transport Equation

The cosmic ray transport equation in the limit of large wave-particle scattering is (Skilling 1971):

$$\frac{\partial f_{\text{p}}}{\partial t} + (\mathbf{u} + \mathbf{v}_{\text{A}}) \cdot \nabla f_{\text{p}} = \nabla \cdot (\kappa_{\text{p}} \mathbf{nn} \cdot \nabla f_{\text{p}}) + \frac{1}{3} p \frac{\partial f_{\text{p}}}{\partial p} \nabla \cdot (\mathbf{u} + \mathbf{v}_{\text{A}}) + Q \quad (17)$$

Here, $f_{\text{p}}(\mathbf{x}, p, t)$ is the cosmic ray distribution function (isotropic in momentum space), u is the gas velocity, \mathbf{v}_{A} is the Alfvén velocity, \mathbf{n} is a unit vector pointing along the magnetic field, and Q is a cosmic ray source function. Throughout this paper, we shall always use the 3D distribution function f_{p} , which does not include the differential volume factor $4\pi p^2$. All momenta p , unless otherwise specified, will always be in units of mc throughout this paper. The actual momentum will be written $\tilde{p}_i = p_i m_i c$, the subscript denoting the particle type. Any distribution functions written as functions of particle energy rather than momentum will be related by

$$dn_i = 4\pi p^2 f_i(p_i) dp_i = f_i(E_i) dE_i \quad (18)$$

$$E_i = \sqrt{1 + p_i^2} m_i c^2 \rightarrow dE_i = \frac{p_i m_i c^2 dp_i}{\sqrt{1 + p_i^2}}$$

Equation (17) is derived from the collisionless Vlasov equation, which expresses conservation of phase space density:

$$\frac{\partial f}{\partial t} + \nabla \cdot (f \mathbf{v}) + \nabla_p \cdot \left(f \frac{\partial \mathbf{p}}{\partial t} \right) = 0 \quad (19)$$

but evaluated in the frame of the Alfvén waves (which has velocity $\mathbf{u} + \mathbf{v}_{\text{A}}$, the sum of the local gas and Alfvén velocities). The distribution function is then expanded in inverse powers of the CR-wave collision frequency ν , $f = f_0 + f_1 + f_2 + \dots$, where $f_r = \mathcal{O}(\nu^{-r})$. Equation (17) is obtained after averaging over pitch angle (justified in the limit of frequent scattering), and is accurate to second order, $\mathcal{O}(\nu^{-2})$. The term with κ_p expresses diffusion relative to the wave frame, and is discussed in detail below. For the details of this expansion we refer the reader to Skilling (1971). This equation implicitly assumes that $f_0 \gg f_1$, i.e. to leading order strong wave-particle scattering renders the distribution function isotropic in the wave frame. As we have seen, for most plasma parameters $(v_{\text{D}} - v_{\text{A}})/c \ll 1$, so this assumption is justified.

The physical interpretation of equation (17) is easy to understand. The left-hand side of this equation is a total time derivative, including an advection term in the frame of the waves. The first two terms on the right-hand side represent diffusion along magnetic field lines relative to the wave frame and adiabatic losses/gains respectively. As long as we have a functional form for κ_p and Q , this equation completely describes the evolution of the cosmic ray population.

Note that in the frame of the wave, and considering the isotropic part of the distribution function f_0 (so that there is no diffusion relative to the wave frame, $\kappa_p = 0$), we have:

$$\frac{Df_0}{Dt} = \frac{1}{3}p \frac{\partial f_0}{\partial p} \nabla \cdot (\mathbf{u} + \mathbf{v}_A) \quad (20)$$

i.e. the CRs evolve adiabatically in the wave frame, with $p \propto n_{\text{CR}}^{1/3}$ (Skilling 1971). This makes physical sense: there are no electric fields in the frame of the wave, and hence the particles conserve energy; they can only scatter in pitch angle. However, the CRs do *not* evolve adiabatically in the frame of the gas, where there are electric fields associated with the hydromagnetic waves. Thus, there is an irreversible energy transfer from the CRs to the gas, with volumetric heating rate (e.g., Kulsrud (2005)):

$$\Gamma_{\text{wave}} = -\mathbf{v}_A \cdot \nabla P_c, \quad (21)$$

which we shall refer to as the “wave heating rate”. This may be thought of as the rate at which work is done on the gas by CR pressure forces, $\mathbf{v}_A \cdot \mathbf{F}$. Importantly, this heating rate is *not* $\Gamma_{\text{wave}} = -\mathbf{v}_D \cdot \nabla P_c$, as has sometimes been adopted elsewhere in the literature (e.g., Uhlig et al. (2012)). The latter expression gives rise to unphysically large heating rates when $v_D \gg v_A$. Super-Alfvénic streaming arises due to a *reduction* in coupling between CRs and gas; it is unphysical that this would give rise to greater heating. Physically, all momentum and energy transfer between the CRs and gas is mediated by hydromagnetic waves; the rate at which work is done by any transmitted forces is therefore set by the velocity of the waves \mathbf{v}_A .

To next order in ν^{-1} , slippage with respect to the wave frame is expressed by the diffusion coefficient κ_p :

$$\kappa(\gamma) = c^2 \left\langle \frac{1 - \mu^2}{\nu(\mu, \gamma)} \right\rangle \quad (22)$$

where the wave-particle collision frequency $\nu(\mu, \gamma)$ is (Kulsrud & Pearce 1969):

$$\nu(\mu, \gamma) = \frac{\pi}{4} \Omega_0 \left(\frac{\delta B}{B} \right)^2 (\mu, \gamma) \quad (23)$$

and the average is taken over pitch angle (Skilling 1971). This expression is obtained from equation (4) as shown by Kulsrud & Pearce (1969), and we assume relativistic CRs such that $v \sim c$. From equation (22), the more frequently CRs interact with Alfvén waves, the more slowly they diffuse relative to the waves— as one might expect, since scattering isotropizes the CR in the wave frame. Equation (23) can be understood from the fact that a single CR-wave encounter in one gyro-period τ leads to a change in pitch angle $\Delta\theta \approx (\delta B/B)$ (Kulsrud 2005); thus $N \sim t/\tau$ encounters leads to a net random walk in pitch angle of $(\Delta\theta)^2 \sim N(\delta B/B)^2 \sim t/\tau(\delta B/B)^2$, or a pitch angle diffusion rate of $D_\theta \sim (\Delta\theta)^2/t \sim \Omega_0(\delta B/B)^2$. Equation (22)

⁶ The mean free path of a CR is roughly the distance over which

can be evaluated by equating wave growth and damping rates to obtain the amplitude of the waves, $(\delta B/B)^2$, as for instance in equation (9). It can also be intuitively written in terms of streaming speeds. From equation (17), we can write the net streaming speed (i.e. the frame in which the mean CR flux vanishes), as (Blandford & Eichler 1987):

$$v_D = \frac{1}{f_p(p)} \left[-\frac{1}{3} v_A p \frac{\partial f_p}{\partial p} - \kappa \mathbf{n} \cdot \nabla f_p \right] \quad (24)$$

where \mathbf{n} is a unit vector pointing along the magnetic field, down the CR gradient. The first term effectively corrects for the Compton-Getting effect, i.e. the differential Doppler shifts of particle energies in transforming from the wave to the inertial frame (depending on whether particles are moving parallel or anti-parallel to the wave, when we calculate the particle flux in the inertial frame, we must compare particles of slightly different energy in the wave frame). If we solve this for the diffusion coefficient, we obtain:

$$\kappa(\gamma) = \frac{f_p}{\mathbf{n} \cdot \nabla f_p} \left[-v_D - \frac{1}{3} v_A \frac{\partial \log f_p}{\partial \log p} \right] \approx L_z [v_D - \frac{3}{2} v_A] \quad (25)$$

Here we have set $\partial \log f_p / \partial \log p \approx -4.5$; as before, the energy dependent CR scale length is $L_z(\gamma) = |f_p / (\mathbf{n} \cdot \nabla f_p)|$. If we insert this into the diffusion term in equation (17), we obtain:

$$D(r) \equiv \nabla \cdot (\kappa_p \mathbf{n} \mathbf{n} \cdot \nabla f_p) \approx \nabla \cdot (f_p \mathbf{n} (v_D - v_A)). \quad (26)$$

where we evaluate the drift speed relative to the wave frame, $(v_D - v_A)$, from equations (10) and (15). Note that the gradient of the distribution function ∇f_p (or equivalently, the scale height L_z) does not appear in the diffusion term. It only appears if $(v_D - v_A)$, has a functional dependence on L_z . This is true for non-linear Landau damping, where $(v_D - v_A) \propto L_z^{-1/2}$ (so that the diffusion term $\propto (\nabla f_p)^{1/2}$ rather than (∇f_p)), but false for turbulent damping, where the diffusion term is therefore *independent* of the magnitude of ∇f .

The latter unusual behavior was first noted by Skilling (1971) for the case of ambipolar damping, which shares similarities with turbulent damping in this regard (although he dismissed it as unimportant, since the effects of diffusion were small for the applications he considered). From equations (22) & (23), and equating wave growth and with a generic damping rate Γ_D , the diffusion term can be expressed more transparently as (Skilling 1971):

$$D(r) = \frac{1}{p^3} \nabla \cdot \left(\frac{\Gamma_D B^2 \mathbf{n}}{4\pi^3 m_p \Omega_0 v_A} \frac{\mathbf{n} \cdot \nabla f_p}{|\mathbf{n} \cdot \nabla f_p|} \right) \quad (27)$$

$$\approx \frac{1}{4\pi^3 p^{7/2} e^{1/2} m_p^{1/2}} \nabla \cdot \left(\frac{B^{3/2} \mathbf{n}}{L_{\text{MHD}}^{1/2}} \frac{\mathbf{n} \cdot \nabla f_p}{|\mathbf{n} \cdot \nabla f_p|} \right) \quad (28)$$

where we specialize to the case of turbulent damping in the second equality, and substitute $\Gamma_{\text{turb}} \approx v_A / (r_L L_{\text{MHD}})^{1/2}$. Note that, other than the sign of $\mathbf{n} \cdot \nabla f_p$, the term within the divergence is independent of f_p . This has important consequences for us, in that diffusion does not slow down with

the pitch angle diffuses by order unity (so that the CR reverses direction), $\lambda \sim c D_\theta^{-1} \sim 3 \times 10^{12} (\delta B/B)^{-2}$ cm, where the pitch angle diffusion coefficient $D_\theta \sim (\delta B/B)^{-2} \Omega_0$. Thus, even small fields of $(\delta B/B) \sim 10^{-3}$ would lead to mean free paths of $\lambda \sim 1$ pc, implying that the diffusive approximation is excellent.

time as ∇f_p decreases. Instead, it is independent of f_p and depends only on plasma properties. If these plasma properties are roughly constant over the streaming timescale, then $\dot{f}_p(r, p, t) \approx D(r, p) \approx$ is roughly constant and $t_{\text{stream}} \propto f_p/f_p \propto f_p$, with decreases with time as f_p falls. This acceleration is key in our more detailed calculations which show that large changes in radio halo luminosity are possible despite apparently long initial diffusion times. It is important to stress, however, that while the diffusion time with turbulent damping is not sensitive to the *magnitude* of ∇f_p , it is still sensitive to the *sign* of ∇f_p . The sign of $\mathbf{n} \cdot \nabla f_p$ reflects the fact that CRs can only stream along B-fields, down their gradient⁷; diffusion has no further effect if $\nabla f_p = 0$. Failure to carefully treat this can result in spurious numerical instabilities (Sharma, Colella & Martin 2010), which we discuss in §3.1.

2.3 Collisional Losses

Cosmic ray protons can also lose energy from direct collisions with gas particles, either through Coulomb interactions, or hadronic interactions (pion production). While these are generally subdominant to losses from wave-particle interactions, we include them for completeness. This transfer of energy from CRs in turn heats the gas.

The energy loss rate of a CR of speed $\beta = v/c$ and kinetic energy E due to Coulomb collisions in ionized gas is: (Mannheim & Schlickeiser (1994))

$$\left(\frac{dE}{dt}\right)_C = -4.96 \times 10^{-19} \text{erg s}^{-1} \left(\frac{n_e}{\text{cm}^{-3}}\right) \frac{\beta^2}{\beta^3 + x_m^3}. \quad (29)$$

Here $x_m = 0.0286[T/(2 \times 10^6 \text{ K})]^{1/2}$, with T and n_e the gas electron temperature and number density. The energy loss rate of a CR due to hadronic collisions is (Mannheim & Schlickeiser (1994)):

$$-\left(\frac{dE}{dt}\right)_h \approx 0.5n_N\sigma_{pp}\beta cE\theta(E - E_{\text{thr}}) \quad (30)$$

where the pp cross section for hadronic interactions is σ_{pp} and the target nucleon density is $n_N = n_e/(1 - 0.5Y)$, Y being the helium mass fraction. The above assumes an inelasticity of $K = 1/2$ for the collision. The Heaviside step function enforces the condition that only cosmic rays with kinetic energy above $E_{\text{thr}} = 282 \text{ MeV}$ undergo pion production. All of the energy loss in Coulomb collisions goes toward heating the gas, whereas only $\sim 1/6$ of the inelastic energy in hadronic collisions goes toward secondary electrons which heat the gas, the rest escaping as gamma rays and neutrinos.

These loss terms are represented in the CR Vlasov equation as:

$$\left(\frac{\partial f_p}{\partial t}\right)_{C,h} = -\frac{\partial}{\partial p}(\dot{p}_{C,h}f_p) \quad (31)$$

$$\dot{p}_{C,h} = \left(\frac{dE(p)}{dt}\right)_{C,h} \left(\frac{dE(p)}{dp}\right)^{-1}$$

⁷ CRs can only stream up a gradient if the sign of energy transfer is reversed – i.e., the gas gives energy to the CRs, rather than vice-versa, as in Fermi acceleration. In this case, the picture of self-confinement is clearly not applicable.

where $E = (\sqrt{1 + p^2} - 1)m_p c^2$ and the momentum p is in units of $m_p c$.

2.4 Turbulent Diffusion

As we have seen, turbulent gas motions can damp MHD waves and enhance CR streaming. However, they can also directly transport CRs advectively. A proper treatment of the interplay between these effects requires 3D MHD simulations. Here, we will simply treat turbulent motions as a diffusive term in the CR transport equation. If $P_{\text{CR}}/P_{\text{gas}}$ is small and CRs have negligible effect on the dynamics, they simply act as a passive tracer species. Analogously to the mixing of metals by turbulent diffusion (Rebusco et al. 2006), we can write:

$$\left(\frac{\partial n_{\text{CR}}}{\partial t}\right)_{\text{turb}} = -\nabla \cdot \left[\kappa_{\text{turb}} n_e \nabla \left(\frac{n_{\text{CR}}}{n_e} \right) \right], \quad (32)$$

where

$$\kappa_{\text{turb}} \approx \frac{v_t L_t}{3} \approx \frac{v_A L_{\text{MHD}}}{3} \quad (33)$$

i.e., if turbulent mixing is vigorous, the CRs will have uniform relative abundance, $n_{\text{CR}} \propto n_e$. This has some support from simulations where CR dynamics are taken into account (Sharma et al. 2009). There, turbulent convection results in constant CR entropy $P/n_{\text{CR}}^{\gamma_{\text{CR}}}$ (where $\gamma_{\text{CR}} = 4/3$) and $P_{\text{CR}}/P_g = \text{const}$. This implies $n_{\text{CR}} \propto P_g^{1/\gamma_{\text{CR}}}$. Since stratified gas in a cluster has a polytropic equation of state $P_g \propto \rho_g^{\gamma_{\text{pt}}}$ where $\gamma_{\text{pt}} \approx 1.2 - 1.3$ (e.g., Capelo, Coppi & Natarajan (2012)), this implies $n_{\text{CR}} \propto (\rho_g)^{\gamma_{\text{pt}}/\gamma_{\text{CR}}} \propto \rho_g^{0.9-0.98}$, consistent with our assumptions. Alternatively, Enßlin et al. (2011) suggest a target profile set by gas entropy, rather than CR entropy: $n_{\text{CR}} \propto P_g^{1/\gamma_g}$, where $\gamma_g = 5/3$. In this case, all occurrences of $n_e(r)$ in equation (32) will be replaced by $\eta(r) = P_g^{1/\gamma_g}$, and $n_{\text{CR}} \propto \rho_g^{\gamma_{\text{pt}}/\gamma_g} \propto \rho_g^{0.72-0.78}$. Given the many uncertainties in the model, this difference in scalings is of secondary importance.

We also need to take adiabatic heating and cooling into account. The normalization of the distribution function f varies with adiabatic changes as $C \propto n_{\text{CR}}^{\alpha/3}$ (e.g., Enßlin et al. (2007)), where $\alpha = 4 - 5$ is the spectral slope of the distribution function. Thus, the overall effect of turbulent diffusion on the distribution function is:

$$\frac{\partial f}{\partial t} = -\nabla \cdot \left[\kappa_{\text{turb}} \delta^{\alpha/3} \nabla \left(\frac{f}{\delta^{\alpha/3}} \right) \right], \quad (34)$$

and $\delta(r) = P_g^{1/\gamma_{\text{CR}}} \approx n_e(r)$, or $\delta(r) = \eta(r) = P_g^{1/\gamma_g}$.

These equations show that turbulent diffusion, acting alone, will lead to a centrally peaked CR profile similar to the gas profile. On the other hand, turbulence also damps MHD waves, leading to enhanced outward streaming, which flattens the CR profile. Which effect dominates? While we explore this in detail in our numerical calculations, it is useful to first get an order of magnitude estimate. From equations (25) and (33), we obtain:

$$\frac{\kappa_{\text{stream}}}{\kappa_{\text{turb}}} \approx \left(\frac{v_D}{v_A} - 1 \right) \left(\frac{L_z}{L_{\text{MHD}}} \right) \propto \frac{1}{L_{\text{MHD}}^{3/2}} \quad (35)$$

We expect $L_z/L_{\text{MHD}} \gtrsim 1$, and $(v_D/v_A - 1) \gtrsim 1$ (from equation (15)) for turbulent damping; moreover, these factors

increase during the streaming processes as L_z rises and n_{CR} fall. Thus, $\kappa_{stream} \gtrsim \kappa_{turb}$ in our fiducial model. Moreover, if the strength of turbulence increases such that L_{MHD} falls, $\kappa_{stream}/\kappa_{turb}$ rises. Stronger turbulence has a larger effect on damping of MHD waves than on inward advection of CRs, and the CRs stream outward faster. Thus, in this framework, turbulent diffusion can never establish a centrally peaked profile, regardless of its strength. In practice, coherent bulk motions (triggered by mergers, or perhaps by gas ‘sloshing’) can potentially bring CRs to the cluster center, and/or produce a magnetic topology which is unfavorable for outward streaming. However, modeling such stochastic events is beyond the scope of this paper.

A few comments about our choice of fiducial parameters for turbulence is in order. It is customary to define (L_t, v_t) , where L_t is the outer scale, and v_t is the velocity at this scale. Instead, we work with (L_{MHD}, v_A) , where L_{MHD} is defined to be the scale at which the turbulent velocity is v_A . In general, $v_t \sim v_A (L_t/L_{MHD})^{1/3}$, and more vigorous turbulence can be characterized by smaller values of L_{MHD} . However, if there is equipartition between $U_B = B^2/8\pi$ and $U_t = 1/2\rho v_t^2$, then $v_t \sim v_A$ and thus $L_t \sim L_{MHD}$. Thus, (L_{MHD}, v_A) are sensible fiducial parameters. Secondly, we have assumed that L_{MHD} (or equivalently, v_t at a fixed scale) is independent of radius. Is this consistent with cosmological simulations, which show that turbulent pressure support becomes increasingly important with radius? A fit to low-redshift clusters gives (Shaw et al. (2010), see also Battaglia et al. (2012)):

$$\left(\frac{P_{turb}}{P_{therm}}\right) = \alpha_0 \left(\frac{r}{R_{500}}\right)^{n_{nt}} \quad (36)$$

where $\alpha_0 \approx 0.18 \pm 0.06$ and $n_{nt} = 0.8 \pm 0.25$. This implies $v_t \propto r^{0.4-\alpha_T/2}$, where $T \propto r^{-\alpha_T}$, and α_T is generally small (e.g., $\alpha_T \approx x^2/(1+1.5x)$) (Loken et al. 2002), where $x \equiv r/r_{vir}$, so $\alpha_T \approx 0.2$ at $r = 0.5r_{vir}$). On the other hand, given our assumption that $B \propto \rho^{\alpha_B}$ (see §3.4), we have $v_A \propto r^{(0.5-\alpha_B)\alpha_\rho}$, where $\rho \propto r^{-\alpha_\rho}$, and $\alpha_\rho \approx 2-3$ over most of the cluster. The radial scalings for v_t and v_A are thus roughly consistent: for instance, $\alpha_B \approx 0.3$ (as assumed for Perseus & Coma) gives $v_A \propto r^{0.4-0.6}$. Finally, we note that for our assumed levels of turbulence, heat dissipation is relatively unimportant. The heating time is:

$$t_{heat} \sim \frac{U_{therm}}{\epsilon} \sim t_{turb} \left(\frac{U_{therm}}{U_{turb}}\right) \sim 5 \text{ Gyr} \frac{f_{t,5} L_{MHD,100}}{v_{A,100}} \quad (37)$$

where $f_{t,5} = [(U_{therm}/U_{turb})/5]$, $L_{MHD,100} = (L_{MHD}/100 \text{ kpc})$, and $v_{A,100} = (v_A/100 \text{ km s}^{-1})$.

3 METHOD

Our main task is to solve the CR transport equation, in the form:

$$\begin{aligned} \frac{\partial f_p}{\partial t} + (\mathbf{u} + \mathbf{v}_A) \cdot \nabla f_p &= \nabla \cdot (\kappa_p \mathbf{nn} \cdot \nabla f_p) \\ &+ \frac{1}{3} p \frac{\partial f_p}{\partial p} \nabla \cdot (\mathbf{u} + \mathbf{v}_A) + Q - \frac{\partial}{\partial p} (\dot{p}_{C,h} f_p) \\ &- \nabla \cdot \left[\kappa_{turb} \delta^{\alpha/3} \nabla \left(\frac{f}{\delta^{\alpha/3}} \right) \right] \end{aligned} \quad (38)$$

where the last two terms are as in equations (31) and (34) respectively. To do so, we have written a new module in a 1D

spherically symmetric version of ZEUS3D, previously used to solve the CR equations in the fluid approximation (Guo & Oh 2008).

Our goal in this paper is to determine if CR streaming is a plausible means of turning off radio halos in the hadronic scenario. We therefore run numerical simulations where the cluster is assumed to be in strict hydrostatic and thermal equilibrium, and only solve the CR transport equation (ignoring the fluid equations for the gas, equations , by setting all time derivatives to zero) to examine the effects of CR streaming. In the absence of a cooling flow, the only time-dependent terms in the fluid equations for the gas (equations (44),(45), and (46)) relate to the CRs, and have negligible effect. We initialize the CR profile so as to reproduce the observed radio surface brightness profiles in the classical hadronic model, and follow the time evolution of radio emission as the CRs stream out. In this methods section, we discuss numerical regularization of CR streaming (§3.1), a test comparison of our CR transport solver in the fluid approximation (§3.2), calculating radio and gamma-ray emission (§3.3), and our initial conditions (§3.4) for a prototypical radio mini-halo (Perseus) and a prototypical giant radio halo (Coma). Results are then presented in the following section, §4.

3.1 CR streaming: Numerical Stability

Cosmic rays can only stream down their gradient, in a direction:

$$\mathbf{s} = -\text{sgn}(\mathbf{B} \cdot \nabla f_p) \frac{\mathbf{B}}{|\mathbf{B}|}. \quad (39)$$

In our 1D simulations, $\mathbf{s} = -\hat{\mathbf{r}} \text{sgn}(df_p/dr)$. However, if this is enforced in equation (28), it leads to numerical instabilities and unphysical oscillations in the distribution function. The origin of this difficulty is easy to understand (Sharma, Colella & Martin 2010); it essentially arises at local extrema. If the simulation at any time produces a local density maximum, diffusion out of the local maximum will cause the density to drop significantly there. If the time step is not properly restricted, this decrease will overshoot, causing the density to drop below neighboring regions, creating a local minimum. The opposite problem will then occur, with inwardly diffusing CRs causing the CR density to increase too much. The result is an unphysical oscillation that eventually spreads out to all space. Because CR streaming results in a flat profile where (df/dr) vanishes everywhere, this problem can become acute as time goes on.

Sharma, Colella & Martin (2010) show that for an explicit code (such as ZEUS3D), the restriction on the time-step such that new local extrema are not created is:

$$\Delta t \leq |f''| \Delta x^3 / f |v| \quad (40)$$

which is much more onerous than the standard Courant condition (we have explicitly verified that simulations which satisfy the Courant condition suffer from spurious oscillations). They suggest regularizing the CR transport equation by replacing the discontinuous $\text{sgn}(f'_p)$ with the smooth function $\tanh(f'_p/\epsilon)$ for some choice of ϵ . As ϵ tends to zero, the tanh function approaches the sign function. This effectively sets ϵ as a minimum scale value for f'_p : if $f'_p \ll \epsilon$, the simulation

behaves as if $f'_p = 0$, and suppresses CR streaming. Alternatively, it can be viewed as introducing a diffusive term at an extremum, with diffusion coefficient f_p/ϵ , similar to the use of explicit viscosity to regularize Euler/Burger's equations. In this case, the maximum time step allowed to suppress the instability is:

$$\Delta t \leq \Delta x^2 \epsilon / 2 f_p |v|. \quad (41)$$

For us, the relevant speed v is the streaming speed, calculated via equation (24), which we insert into this equation.

We have found that a scale value of:

$$\epsilon = f_p / L; \quad L = 3 \text{ Mpc} \quad (42)$$

is sufficiently small that decreasing it any further does not significantly change the results. In Fig 1, we show a convergence test (showing the radio luminosity of Perseus as a function of time when $L_{\text{MHD}} = 100 \text{ kpc}$; see Fig 3b) where the figure converges to the correct solution as ϵ is decreased; a value of ϵ half of our fiducial value ($\epsilon = 10^{-25} f_p$) gives identical results.

In practice, although we use a smoothing scale ϵ , we use the time constraint (40) rather than (41) and we use $v = v_A$ rather than $v = v_s$. Additionally, to prevent the time step from dropping to zero we impose a minimum time step

$$\Delta t \geq 1 \times 10^{-7} \Delta x^2 \epsilon / 2 f_p |v| \quad (43)$$

where the numerical factor out front is arbitrary. We do all of this to regulate the runtime of the simulation - the less stringent time steps will be less accurate but will run quicker, and we can adjust the minimum time step (43) to the desired balance of speed and accuracy. As a result, local minima and maxima do develop at some points of our simulations, however this will always happen as the CR profile flattens; as long as the local extrema do not grow unstably the results should be robust.

In addition, we enforce the constraint that $\Delta f_p \leq 0.05 f_p$ in a single time-step (and similarly for the gas energy and density). Note that while (40) is only applied at local extrema, this condition is held everywhere. Eventually, as f_p falls, this shrinks the time-step to zero. To avoid this, we define a momentum dependent minimum $f_{p,\text{min}}(p) = 10^{-3} f_p(r_{\text{max}}, p, t_0)$, where r_{max} is the outer boundary of the simulation, and t_0 is the initial time. The distribution function f_p is then never allowed to drop below this value. Also, once f_p falls below $50 f_{p,\text{min}}(p)$ anywhere, all time step restrictions there are ignored, including (40).

3.2 Test Case: AGN Feedback

To test our solver for the CR transport equation, it is useful to compare against previous results where CRs are treated in the fluid approximation. Specifically, we compare against the results of Guo & Oh (2008), which simulates the effects of CRs injected by a central AGN on the thermal state of a cool core cluster. It was found that a combination of electron thermal conduction (at some fraction f of the Spitzer value) and CR mediated wave heating was sufficient to stem a cooling flow. The following governing equations for the two-fluid ICM (gas and cosmic rays) were used:

$$\frac{\partial \rho}{\partial t} + \nabla \cdot (\rho \mathbf{u}) = 0 \quad (44)$$

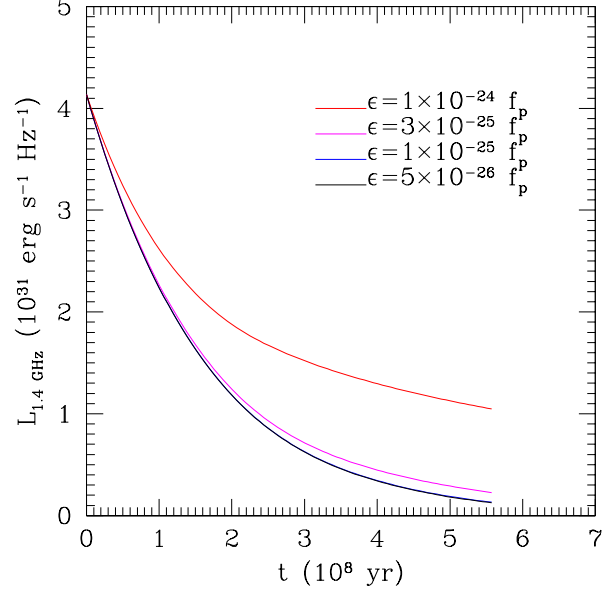


Figure 1. Convergence test for the smoothing scale parameter ϵ . We plot the 1.4 GHz radio luminosity of Perseus, which declines with time due to cosmic-ray streaming (here we assume $L_{\text{MHD}} = 400 \text{ kpc}$; see §4.1 for details). As ϵ is decreased, our calculations converge. Our fiducial value is $\epsilon = 10^{-25} f_p$.

$$\frac{\partial \mathbf{S}}{\partial t} + \nabla \cdot (\mathbf{S} \mathbf{u}) = -\nabla P_g - \nabla P_c - \rho \nabla \Phi \quad (45)$$

$$\begin{aligned} \frac{\partial E_g}{\partial t} + \nabla \cdot (E_g \mathbf{u}) = & -P_g \nabla \cdot \mathbf{u} - \nabla \cdot \mathbf{F} \\ & - n_e^2 \Lambda(T) + \eta_c n_e E_c - \mathbf{v}_A \cdot \nabla P_c \end{aligned} \quad (46)$$

$$\frac{\partial E_c}{\partial t} = (\gamma_c - 1)(\mathbf{u} + \mathbf{v}_A) \cdot \nabla E_c - \nabla \cdot \mathbf{F}_c + Q_c. \quad (47)$$

$$\mathbf{F}_c = \gamma_c E_c (\mathbf{u} + \mathbf{v}_A) - \mathbf{n} \kappa_c (\mathbf{n} \cdot \nabla E_c), \quad (48)$$

where ρ is the gas density, P_g is the gas pressure, E_g is the gas energy density, $\mathbf{S} = \rho \mathbf{u}$ is the gas momentum vector, E_c is the cosmic ray energy, $P_c = (\gamma_c - 1) E_c$ is the cosmic-ray pressure, \mathbf{F} is the electron conduction heat flux, and Φ is the gravitational potential. The term $\eta_c n_e E_c$, where $\eta_c = 2.63 \times 10^{-16} \text{ cm}^3 \text{ s}^{-1}$, takes Coulomb and hadronic heating of the gas by cosmic rays into account. The initial conditions, gravitational potential $\Phi(r)$, and cooling function $\Lambda(T)$ are as spelled out in Guo & Oh (2008); please refer to the paper for details. The source function Q represents the injection of CRs by an AGN, triggered by gas cooling:

$$Q_c = -\frac{\nu \epsilon \dot{M}_{\text{in}} c^2}{4\pi r_0^3} \left(\frac{r}{r_0}\right)^{-3-\nu} [1 - e^{-(r/r_0)^2}] \quad (49)$$

Here, $\epsilon = 3 \times 10^{-3}$ is an efficiency parameter, $\nu = 0.3$, and $r_0 = 20 \text{ kpc}$ is a scale distance.

The code of Guo & Oh (2008) uses the CR energy density E_c as the fundamental dynamic variable for CRs. It is:

$$E_c = 4\pi \int_0^\infty p^2 T_p(p_p) f_p(p_p) dp \quad (50)$$

where

$$T_p(p) = \left[\sqrt{1 + p^2} - 1 \right] mc^2. \quad (51)$$

is the kinetic energy of a CR proton of momentum p_p . By using E_c as the main CR dynamic variable, all momentum dependence has been integrated out. By contrast, we wish to retain momentum dependence, and instead use $f(r, p, t)$ as our fundamental variable. We therefore continue to solve equations (44) – (46), but replace equations (47) & (48) with the equation for the distribution function, equation (38), and solve for E_c as required in equations (45), (46) via equations (50) and (51). In calculating the momentum-dependent source function Q for use in equation (38), we suppose that the injected spectra has the form:

$$f_p(E) = \frac{A_{cr}\theta(E - E_1)}{(E/E_*)^{\tilde{\alpha}} + (E/E_*)^{(\tilde{\alpha}-2)/2}} \quad (52)$$

which assumes a steady state spectrum at low (high) energies due to Coulomb (hadronic) losses, and smoothly connects these regimes (see (Guo & Oh 2008) for details). Here, $E_* = 706$ MeV is a cross-over energy separating the low- and high-energy regimes, while the assumed spectral index is $\tilde{\alpha} = 2.5$, and cutoff energy is $E_1 = 10$ MeV. We create a source function with the same momentum dependence as equation (52), and then normalize it to the total CR injection rate given by equation (49):

$$Q_c = 4\pi \int_0^\infty p^2 T_p Q dp. \quad (53)$$

To maintain consistency with Guo & Oh (2008), we use the same momentum-independent diffusion coefficient used there.

The simulation grid has two ghost zones at each end in the radial direction, and one ghost zone at each end in the momentum direction. The density and temperature of the ICM are linearly extrapolated into the spatial ghost zones. For the CR spectrum, constant boundary conditions are enforced in the radial direction, i.e. $f_p(p)$ at the spatial ghost zones are set equal to $f_p(p)$ in the adjacent active zones. In the momentum direction we required that $d \log f_p / d \log p$ be constant across the boundary. As for time step constraints, for this test case we do not allow ρ_g or E_g to change by more than 25% in any time step. We also enforce the Courant condition for all cells, $\Delta t < \Delta x^2 / 2\kappa_p$.

We find that our full model reproduces the results of Guo & Oh (2008) extremely well. An example is shown in Fig. 2, where we show the temperature as a function of time for several select radii. The cluster is initialized to be isothermal; after an initial transient, it is thermally stabilized against a cooling catastrophe by a combination of CR heating and electron thermal conduction. The dotted lines show the results from the code of Guo & Oh (2008), which integrates the fluid equations, while the solid lines indicate the results of the new code, which computes the distribution function. Indeed, even when we include the full momentum dependence of the diffusion coefficient, the results barely change (for this particular example, we have assumed non-linear Landau damping). This is because most of the energy density of CRs is dominated by low energy CRs (~ 1 GeV) for which the diffusion time is negligibly long. As we shall soon see, diffusion cannot be neglected for the high-energy CRs which are responsible for observed radio emission.

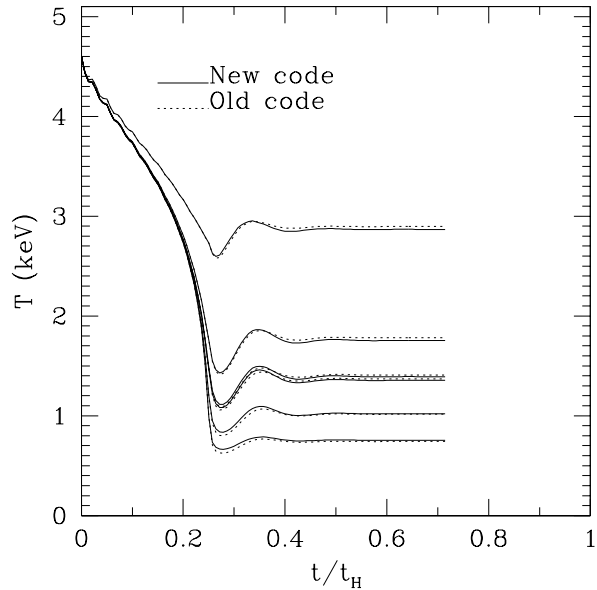


Figure 2. Temperature versus simulation time at some select radii for the new code, where we solve the CR transport equation (38). The results of the old code, which treats CRs in the fluid limit (equations (47), (48)), are displayed in the dotted lines.

3.3 Computing Emissivities

Our fundamental simulation variable is the CRp distribution function, $f_p(r, p, t)$. Here, we describe how radio and gamma-ray emission can be inferred from $f_p(p)$ (hereafter, we suppress r, t) in the hadronic model, given an assumed gas density and magnetic field.

How is radio emission produced? CR protons undergo hadronic interactions to produce pions, which in turn decay to produce relativistic electrons (CRp + nucleon $\rightarrow \pi^\pm, \pi^0$; $\pi^\pm \rightarrow \mu^\pm + \nu_\mu / \bar{\nu}_\mu \rightarrow e^\pm + \nu_e / \bar{\nu}_e + \nu_\mu + \bar{\nu}_\mu$; $\pi^0 \rightarrow 2\gamma$). The high energy electrons which produce observable synchrotron emission have short cooling lifetimes and we therefore assume a steady-state between injection and cooling. A CRp distribution $f_p(p)$ gives rise to a pion source function due to the hadronic pp interaction (Pfrommer, Enßlin & Springel 2008):

$$s_{\pi^\pm}(p_\pi) = \frac{2}{3} \int_{-\infty}^{\infty} dp_p f_p(p_p) c n_N \xi(p_p) \sigma_{pp}^\pi \times \delta\left(p_\pi - \frac{m_p}{4m_\pi} p_p\right) \theta(p_p - 0.78) \quad (54)$$

where $\sigma_{pp}^\pi = 32(0.96 + e^{4.4-2.4\alpha_p})$ mbarn⁸. The delta function enforces the mean pion momentum $\langle \tilde{p}_\pi \rangle = \tilde{p}_p/4$ and the Heaviside step function θ incorporates the threshold proton momentum for the pion production to occur. Approximating

⁸ We follow Pfrommer & Enßlin (2004) in absorbing the weak energy dependencies of the pion multiplicity and the inelastic cross-section in this semi-analytical parametrization of the cross-section, where α_p is the average CR spectral index.

the pion multiplicity ξ as 2, this gives:

$$s_{\pi^\pm}(p_\pi) = \frac{16}{3} \frac{m_\pi}{m_p} c_{N\sigma} \sigma_{pp}^\pi 4\pi \left(\frac{4m_\pi}{m_p} p_\pi \right)^2 \times f_p \left(\frac{4m_\pi}{m_p} p_\pi \right) \theta \left(\frac{4m_\pi}{m_p} p_\pi - 0.78 \right) \quad (55)$$

Under this approximation, the neutral pion source function s_{π^0} is the same.

The charged pion population will undergo pion decay, producing electrons (and other particles). This electron production is described with the electron source function:

$$s_e(p_e) = s_{\pi^\pm}(p_\pi(p_e)) \frac{dp_\pi}{dp_e} \quad (56)$$

$$\Rightarrow s_e(p_e) = \frac{64}{3} \frac{m_e}{m_p} c_{N\sigma} \sigma_{pp}^\pi 4\pi \left(\frac{16m_e}{m_p} p_e \right)^2 \times f_p \left(\frac{16m_e}{m_p} p_e \right) \theta \left(\frac{16m_e}{m_p} p_e - 0.78 \right) \quad (57)$$

In the second equation we have used $\tilde{p}_\pi = 4\tilde{p}_e$. If we assume an equilibrium between this source and any losses, i.e. a steady state solution, the electron spectrum is then determined from

$$f_e(p_e) = \frac{1}{|\dot{p}_e|} \int_{p_e}^{\infty} dp'_e s_e(p'_e) \quad (58)$$

where the losses \dot{p}_e are

$$\dot{p}_e(p_e) = \frac{\dot{E}_e}{m_e c^2} = \frac{4}{3} \frac{\sigma_T c p_e^2}{m_e c^2} (\varepsilon_B + \varepsilon_{\text{cmb}}) \quad (59)$$

from synchrotron radiation and inverse Compton (IC) scattering. Here, σ_T is the Thompson scattering cross section, and $\varepsilon_B, \varepsilon_{\text{cmb}}$ are the energy density of the B-field and cosmic microwave background.

From the electron distribution function we can determine the resulting synchrotron emissivity (Rybicki & Lightman 1979):

$$j_\nu(r) = 0.333 \frac{\sqrt{3}}{2\pi} \frac{e^3 B(r)}{m_e c^2} \int_1^\infty d\gamma_e f_e(r, \gamma_e) F \left(\frac{\nu}{\nu_c} \right) \quad (60)$$

In the above, $\nu_c = 3eB\gamma_e^2/4\pi m_e c$ and the function F is an integral of a modified Bessel function, $F(x) = x \int_x^\infty K_{5/3}(x') dx'$. The numerical factor in front comes from averaging the CRe population over pitch angle, assuming isotropy. The observed surface brightness is:

$$S_\nu(r_\perp) = \int_{-\infty}^{\infty} j_{\nu'}(r(l)) dl = \frac{2}{(1+z)^3} \int_{r_\perp}^{\infty} j_{\nu'}(r) \frac{r dr}{\sqrt{r^2 - r_\perp^2}} \quad (61)$$

where $\nu' = \nu(1+z)$. The luminosity is:

$$L_\nu = \int d^3\mathbf{r} j_\nu(r) \quad (62)$$

We also make predictions for gamma-ray emission. We only consider gamma-ray emission from neutral pion decay $\pi^0 \rightarrow 2\gamma$ and ignore the subdominant contribution from inverse Compton scattering. The analysis is much the same as above. Following Mannheim & Schlickeiser (1994), we derive a photon source function from the pions:

$$s_\gamma(E_\gamma) = 2 \int_{E_\gamma + \frac{(m_\pi c^2)^2}{E_\gamma}}^{\infty} \frac{dE_\pi s_{\pi^0}(E_\pi)}{\sqrt{E_\pi^2 - m_\pi^2 c^4}} \quad (63)$$

where the neutral pion source function $s_{\pi^0}(E_\pi)$ is assumed to be the same as for charged pions, equation (55). From this source function, we determine a number production rate per unit volume λ_γ :

$$\lambda_\gamma(> E_\gamma) = \int_{E'_\gamma}^{\infty} dE'_\gamma s_\gamma(E'_\gamma) \quad (64)$$

and the flux detected at Earth above an energy E_γ :

$$F_\gamma(> E_\gamma) = \frac{1}{4\pi d_L^2} \int d^3\mathbf{r} \lambda_\gamma(> E_\gamma) \quad (65)$$

Given the strong momentum dependence of CR streaming, it is worth clarifying which range of CRp momenta are most observationally relevant. For radio emission, the characteristic synchrotron frequency is $\sim 3\gamma^2\nu_c$, where ν_c is the non-relativistic synchrotron frequency. For a given observational frequency ν_s , the greatest contribution comes from electrons with:

$$p_{\text{emit}} \approx \gamma_{\text{emit}} \approx 4 \times 10^3 \left(\frac{\nu_s}{1 \text{ GHz}} \right)^{1/2} \left(\frac{B}{3 \mu\text{G}} \right)^{-1/2} \quad (66)$$

Thus, ~ 10 GeV electrons are responsible for \sim GHz emission in μG fields. Typically, $\tilde{p}_e \sim (1/16)\tilde{p}_p$, where \tilde{p}_e is the momentum of a secondary CRe produced hadronically. The reduction in energy by a factor of ~ 16 comes from the fact that the limiting inelasticity is $\sim 1/2$ (Mannheim & Schlickeiser 1994), the pion multiplicity is a factor of ~ 2 due to 2 pion jets leaving the interaction site (Nachtmann 1990), and $\langle E \rangle = (1/4)\langle E_{\pi^\pm} \rangle$ in the reaction $\pi^\pm \rightarrow e^\pm + 3\nu$. Thus for \sim GHz emission, ~ 100 GeV protons are most relevant, while for LOFAR observations at ~ 100 MHz, ~ 10 GeV protons are most relevant. For γ -ray emission, $E_\gamma \approx (1/8)E_p$ (all the factors are as before, except $E_\gamma = 1/2E_{\pi^0}$). Thus, Fermi, which is most sensitive in the $E_\gamma \approx 0.1 - 3$ GeV range (rather than 0.1 - 300 GeV, due to the pion bump), probes $E_p \sim 1 - 30$ GeV, while imaging air Cerenkov telescopes such as MAGIC, HESS and VERITAS are most sensitive in the $E_\gamma \sim 0.3 - 1$ TeV range (rather than 0.3-10 TeV, due to the steep CRp spectrum), probes $E_p \sim 3 - 10$ TeV.

3.4 Initial and Boundary Conditions

We choose to simulate a prototypical radio mini-halo, Perseus, and a prototypical giant radio halo, Coma. We choose initial conditions which reproduce current observations of their radio surface brightness, and then watch how this evolves under the influence of streaming. For the Perseus cluster, we adopt empirical fits to the cluster temperature and electron density profiles (Pinzke & Pfrommer (2010)) based on observed X-ray emission (Churazov et al. (2003)):

$$\frac{n_e}{10^{-3} \text{ cm}^{-3}} = 46 \left[1 + \left(\frac{r}{57 \text{ kpc}} \right)^2 \right]^{-1.8} + 4.79 \left[1 + \left(\frac{r}{200 \text{ kpc}} \right)^2 \right]^{-0.87} \quad (67)$$

$$T = 7 \text{ keV} \frac{1 + (r/71 \text{ kpc})^3}{2.3 + (r/71 \text{ kpc})^3} \left[1 + \left(\frac{r}{380 \text{ kpc}} \right)^2 \right]^{-0.32} \quad (68)$$

From these we determine an internal energy distribution (via the ideal gas law) and a gravitational potential (via hydrostatic equilibrium). Similarly, for Coma the fits are (Pinzke & Pfrommer (2010), based on Briel, Henry & Boehringer (1992)):

$$\frac{n_e}{10^{-3}\text{cm}^{-3}} = 3.4 \left[1 + \left(\frac{r}{294 \text{ kpc}} \right)^2 \right]^{-1.125} \quad (69)$$

$$T = 8.25 \text{ keV} \left[1 + \left(\frac{r}{460 \text{ kpc}} \right)^2 \right]^{-0.32} \quad (70)$$

The radio surface brightness profiles at 1.4 GHz are fit by a β profile:

$$S(r) = S_0 [1 + (r/r_c)^2]^{-3\beta+0.5} \quad (71)$$

which is reproduced by an initial emissivity of

$$j_\nu(r) = j_{\nu,0} [1 + (r/r_c)^2]^{-3\beta} \quad (72)$$

$$j_{\nu,0} = \frac{S_0}{2\pi r_c} (6\beta - 1) \mathcal{B} \left(\frac{1}{2}, 3\beta \right)$$

where \mathcal{B} is the beta function. For Perseus, $\beta = 0.55$, $r_c = 30$ kpc, and $S_0 = 2.3 \times 10^{-1}$ Jy arcmin $^{-2}$ (Pedlar et al. 1990), while for Coma $\beta = 0.78$, $r_c = 450$ kpc, and $S_0 = 1.1 \times 10^{-3}$ Jy arcmin $^{-2}$ (Deiss et al. 1997).

We assume that the magnetic field scales with gas density:

$$B = B_0 \left(\frac{n_e(r)}{n_e(0)} \right)^{\alpha_B} \quad (73)$$

Such a scaling is motivated by simulations (Dubois & Teyssier 2008) and Faraday rotation measurements (Bonafede et al. 2010; Kuchar & Enßlin 2011); for instance, rotation measurements for Coma are well fit by $\alpha_B \approx 0.3 - 0.7$ (Bonafede et al. 2010). In the future it would be interesting to explore other scalings, if for instance this relationship also has temperature dependence (Kunz et al. 2011). We find that radio surface brightness profiles can be well fit by $\alpha_B = 0.3$ for both clusters, but for Perseus $B_0 = 10 \mu\text{G}$, while for Coma $B_0 = 5 \mu\text{G}$. We choose a cosmic ray distribution function motivated by cosmological hydrodynamic simulations of galaxy clusters where cosmic rays are accelerated via diffusive shock acceleration (Pinzke & Pfrommer 2010):

$$f_p(r, p_p) = C(r) \sum_i \Delta_i p_p^{-\alpha_i} \quad (74)$$

$$\Delta = (0.767, 0.143, 0.0975) \quad \alpha = (2.55, 2.3, 2.15). \quad (75)$$

and the normalization

$$C(r) = \frac{(C_{\text{vir}} - C_{\text{center}})}{1 + \left(\frac{r}{r_{\text{trans}}} \right)^{-\beta_C}} + C_{\text{center}}. \quad (76)$$

Note that these simulations do not take into account the effects of cosmic ray streaming. The parameters $C_{\text{vir}}, C_{\text{center}}, r_{\text{trans}}$ are then chosen such that the model radio brightness profile agrees with fits to observations (equation (3.4)). For Perseus, if we define $C(r) = \tilde{C}(r)n_e(r)$, then $\tilde{C}_{\text{center}} = 8.3 \times 10^{-8}$, $\tilde{C}_{\text{vir}} = 7.2 \times 10^{-8}$, $r_{\text{trans}} = 36$ kpc, $\beta_C = 1.0$. For Coma, $C_{\text{center}} = 6 \times 10^{-11} \text{ cm}^{-3}$,

$C_{\text{vir}} = 5.2 \times 10^{-11} \text{ cm}^{-3}$, $r_{\text{trans}} = 55$ kpc, $\beta_C = 1.09$. The initial radio surface brightness profiles derived from these parameters are shown in Fig 3a and 5a.

When we solve equation (38), the simulation grid has two ghost zones at each end in the radial direction, and two ghost zones at each end in the momentum direction. To set values in the ghost zones, we use $d \log f_p / d \log p = \text{const}$ in the momentum direction at both the inner and outer boundary, i.e. a power law extrapolation. In the spatial direction, we use $d \log f_p / d \log r = \text{const}$ at the inner boundary. The outer boundary requires a little more care, since it can fall to extremely low values which result in round-off error; also, if the CR gradient goes to zero at the outer simulation boundary, this artificially suppresses CR streaming. For Perseus, we use $d \log f_p / d \log r = \text{const}$ at the outer boundary, but subject to the condition that $f_{\text{min}} \leq f_{i_{\text{max}}+1} \leq X f_{i_{\text{max}}}$, $f_{\text{min}} \leq f_{i_{\text{max}}+2} \leq X f_{i_{\text{max}}+1}$, where i_{max} is the index of the last active zone, $f_{\text{min}}(p) = 10^{-3} f_p(r_{\text{max}}, p, t_0)$, and $X = 0.98$. For Coma, where the initial profile is already extremely flat, we simply adopt $f_{i_{\text{max}}+1} = X f_{i_{\text{max}}}$, $f_{i_{\text{max}}+2} = X f_{i_{\text{max}}+1}$. To conserve CRs during the process of turbulent advection, we also enforce the CR turbulent diffusion flux, defined as $\mathbf{F}_{\text{turb}} = \kappa_{\text{turb}} \delta^{\alpha/3} \nabla (f_p \delta^{-\alpha/3})$ (see equation (34)), to be zero at both spatial boundaries.

For both Perseus and Coma, we use 1.4 GHz data. Note that for Coma, which is the most well-studied giant radio halo, recent 1.4 GHz and 352 MHz data cannot be reconciled by the classical hadronic model with a power-law spectrum (Brown & Rudnick 2011), though this conclusion is subject to systematic uncertainties in the zero-point of 1.4 GHz data (Zandanel, Pfrommer & Prada 2012). We shall also see that energy dependence in the streaming speed alters the CR distribution function, so that it is no longer a power-law in momentum, potentially solving this problem.

4 RESULTS

We now show results for a canonical radio mini-halo in a cool core cluster (Perseus), and giant radio halo in a non-cool core cluster (Coma), starting from the initial conditions given in §3.4. We use Perseus to illustrate most of the relevant physics. Unless otherwise noted, all calculations assume $L_{\text{MHD}} = 100 \text{ kpc}$, where L_{MHD} is the lengthscale at which $v_A = v_{\text{turb}}$ (note from $\epsilon = v_A^3 / L_{\text{MHD}}$ that smaller values of L_{MHD} correspond to more vigorous turbulence).

4.1 Perseus Cluster

The initial conditions for Perseus correspond to a CR profile where the ratio of CR energy to the thermal gas energy is almost constant throughout the cluster, decreasing slightly in the outskirts. In Fig 3a we compare radio emission from our initial conditions to surface brightness observations at 1.4 GHz from Pedlar et al. (1990). Note that the observations only span a limited radial range (which produces $\sim 1/2$ of the total radio luminosity in our model). The normalization of the profile falls substantially in several hundred Myr,

while its shape does not evolve significantly⁹. Fig 3b shows the evolution of the 1.4 GHz radio luminosity with time, and how it depends on the strength and nature of loss processes. The fall in luminosity is exponential, on a characteristic $\sim 10^8$ yr timescale. For our fiducial $L_{\text{MHD}} = 100$ kpc simulation, $L_{1.4\text{GHz}}$ falls by an order of magnitude in several hundred Myr; the decrease is faster for smaller values of L_{MHD} , which corresponds to strong damping. If only non-linear Landau damping operates, the decline in luminosity is very slow, and insufficient to turn off radio halos. We also show how $L_{1.4\text{GHz}}$ evolves if we ignore diffusion (i.e., the no damping limit) or adiabatic losses in equation (38).

The streaming speeds relative to the wave frame for 100 GeV CRps at a radius of 100 kpc are shown in figure 3c, for different values of L_{MHD} and if only non-linear Landau damping dominates. We see that even if the streaming speeds start out slow, they can quickly become super-Alfvénic as the CR density drops. This non-linear behavior, which is due to the unusual $\kappa \propto 1/\nabla f$ scaling of the diffusion coefficient for turbulent damping, allows very fast streaming. It is not seen if only non-linear Landau damping operates; in that case, $v_{\text{D}} \sim \mathcal{O}(v_{\text{A}})$ at all times. Note from equation (7) that $v_{\text{D}} - v_{\text{A}} \sim (\lambda/3L_{\text{z}})c$. Thus, as $v_{\text{D}} \rightarrow c$, $\lambda \rightarrow L_{\text{z}}$, and our equations break down, as the CRs can no longer be described by a distribution function. Instead, a fully kinetic approach is needed. This limitation is relatively unimportant since by this stage CRs are no longer self-confined but stream freely along field lines; thus, turn-off is extremely rapid.

The individual contributions to \dot{f}_{p} at 100 GeV are shown in Figure 3d in the $L_{\text{MHD}} = 100$ kpc case. The values are taken at a fixed radius of 100 kpc, and displayed as a function of time. Interestingly, no one process dominates (and we have verified that adiabatic and diffusive losses acting in tandem are much more effective than either process alone). Initially, adiabatic losses dominate, although they decrease continuously with time. This is to be expected, since the adiabatic loss term is proportional to f_{p} , and decreases as f_{p} falls. On the other hand, the diffusion loss term from turbulent damping is independent of f_{p} (equation (28)), and thus independent of time as long as there is a spatial gradient. At $t \sim 190$ Myr, the profile at $r \sim 100$ kpc flattens (see Fig. 3e), and all terms plummet, although the adiabatic loss term falls most drastically. In §5, we explore the nature of this change when the profile flattens: inside the flat core, \dot{f}_{p} changes since it is determined solely by the flux at the outer boundary of the core. From this plot, we can see why adiabatic and diffusive losses in tandem are much more efficient than either alone: adiabatic losses are much more effective in the early stages when the profile is centrally peaked, while diffusive losses are more effective once the profile flattens. We also see that inward turbulent advection is non-negligible but subdominant. It also changes once the region becomes incorporated inside the flat core (since once again only the flux through the core boundary matters at that point).

Fig 3e shows $4\pi r^3 \dot{f}_{\text{p}}$ (i.e., CR density) for 100 GeV CRs. As previously discussed, the CR density profile develops a flat core, which expands in size at roughly the streaming

speed. Meanwhile, the normalization of the CR profile falls continuously, even for the flat portion. The end result is a profile in which the CR profile has completely flattened and fallen by several orders of magnitude by the end of the simulation.

Finally, the expected γ -ray flux as calculated from equation (65) is shown in Fig 3f. Observed upper limits are also shown; note that our initial conditions are consistent with these upper limits. Due to the finite momentum grid $p_{\text{p}} \leq 5000$, our calculations are only accurate in the range $E_{\gamma} \lesssim 200$ GeV, although the high energy CRs stream so quickly that the CR transport equation quickly breaks down, in any case. The gamma-ray fluxes decline extremely rapidly with time, with the decline being much sharper at higher energies, due to the fact that higher energy CRs stream faster. The upshot is that at the $E_{\gamma} \sim 0.3 - 1$ TeV ($E_{\text{CR}} \sim 3 - 10$ TeV) energies probed by imaging air Cherenkov telescopes (MAGIC, HESS, VERITAS), the decline in gamma-ray luminosity is very rapid. Any detection of gamma-ray emission at these energies, where a source is not immediately apparent (suggesting that it is long-lived), would strongly disfavor the model of CR streaming presented here. However, the $E_{\gamma} \sim 0.1 - 3$ GeV ($E_{\text{CR}} \sim 1 - 30$ GeV) energies probed by Fermi correspond to CRs which stream and turn off gamma-ray emission more slowly. The latter is thus a more robust measure of the cluster's CR injection history. Note that since $\langle E_{\gamma} \rangle \sim 1/8 \langle E_{\text{CR}} \rangle$, gamma-ray emission at $E_{\gamma} \sim 10$ GeV corresponds to the $E_{\text{CR}} \sim 100$ GeV CRs relevant for \sim GHz radio emission, and declines by a similar amount.

By the same token, the energy dependence of CR streaming implies that radio luminosity turns off more slowly at lower frequencies. We show this in Fig 7. We can also see this in figure 4 which plots the distribution function versus momentum. The higher energy CRps drop in density much faster than lower energy CRps. The corresponding high energy synchrotron emission then also drops faster. This behavior could explain radio halos such as Abell 521, which is detected at 240, 325 and 610 MHz, but not at 1.4 GHz, implying a cutoff or strong spectral curvature at high frequencies (Brunetti et al. 2008). We therefore predict that at the low frequencies probed by LOFAR, radio halos should be significantly more abundant.

4.2 Coma Cluster

We now turn to Coma, a prototypical giant radio halo. We focus on the differences with our previous example, Perseus. Due to the flat and extended observed surface brightness profile, which extends out to 1 Mpc (Fig 5a, observations from Deiss et al. (1997)), the inferred CRp distribution is much flatter. Indeed, for the B-field we have assumed, $B \propto \rho^{\alpha_{\text{B}}}$, $\alpha_{\text{B}} \approx 0.3$ (which is consistent with rotation measure observations (Bonafede et al. 2010)), the radio profile can be fit by a nearly flat CRp density (Fig. 5e). This large flat inferred profile is suggestive that extensive streaming has already taken place. Coma thus presents an interesting challenge, to see if a significant decline in luminosity is possible despite the absence of significant CR gradients except a small one at the outer boundary. We emphasize once again that for turbulent wave damping, our solutions are indepen-

⁹ This is mostly due to projection effects; note that the CR radial profile *does* evolve significantly; see Fig. 3e.

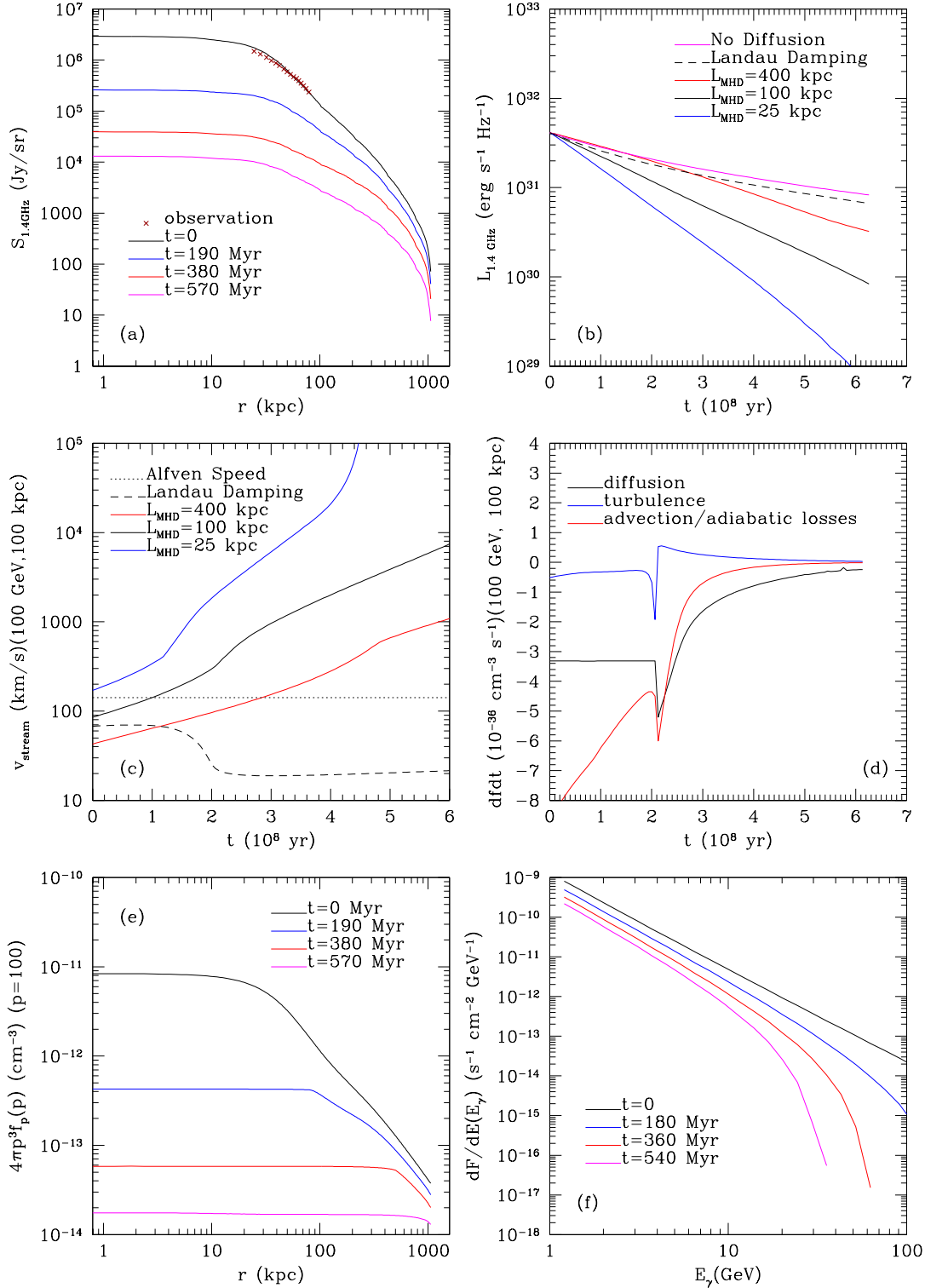


Figure 3. Simulation results for the Perseus cluster. **(a)** Radio surface brightness of Perseus for $L_{\text{MHD}} = 100$ kpc. Observations from Pedlar et al. (1990). **(b)** The time evolution of the Perseus cluster’s radio luminosity for different levels of damping. The solid lines show MHD turbulence damping at various strengths. The dashed line shows non-linear Landau damping. **(c)** Cosmic ray streaming speeds of 100 GeV CRs at a fixed radius of 100 kpc. **(d)** Different contributions to \dot{f}_p for the $L_{\text{MHD}} = 100$ kpc Perseus simulation. **(e)** Radial distribution of 100 GeV protons for $L_{\text{MHD}} = 100$ kpc. **(f)** Predicted gamma-ray fluxes. Upper limits from observations are at higher energies than those plotted here.

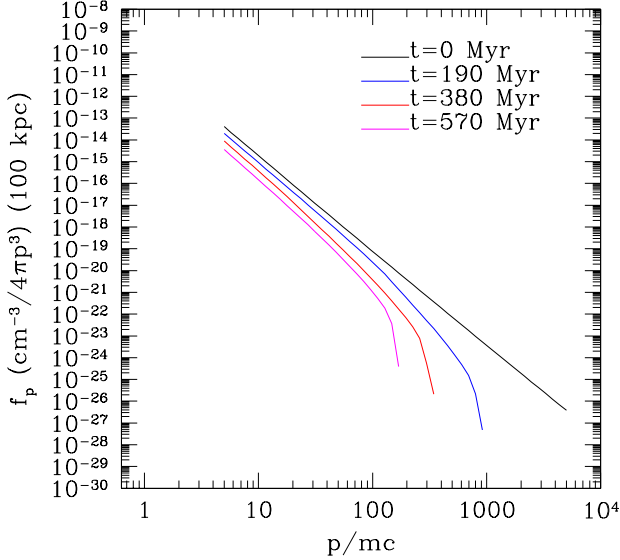


Figure 4. CR distribution function versus momentum at a fixed radius of 100 kpc. The dropoff time scales with energy, leading to the spectral steepening discussed above.

dent of the magnitude of the CR gradient ∇f . Our solutions depend only on where ∇f is non-zero, and its sign.

We show our results in Fig. 5. All figures are analogs of those for Perseus in Fig. 3 (except we adopt $r=300$ kpc as our fiducial radius when displaying time-varying quantities—due to the much larger extent of the Coma radio halo, this is a more representative radius), and we again adopt $L_{\text{MHD}} = 100$ kpc for our fiducial model. In Fig 5a, we see that the surface brightness falls in normalization, but does not significantly change shape, as for Perseus. The decline in $L_{1.4\text{GHz}}$ is slower than for Perseus, although $L_{1.4\text{GHz}}$ is still down by an order of magnitude after ~ 600 Myr for the fiducial model, and declines more quickly with more vigorous turbulence as expected. Non-linear Landau damping alone produces a slow decline. While streaming is super-Alfvénic (Fig 5c), it does not ‘run away’ with time as quickly as for Perseus. The acceleration of CR streaming is tied to the decline of the CR density, which is slower in this case.

Since the flat region encompasses the entire cluster at the outset, there is no transition in energy loss regimes as for Perseus (where the profile gradually flattens). Instead, loss rates vary mildly with time (Fig 5d), with diffusive losses always more important than adiabatic losses, which are essentially negligible. This can be understood from the fact that adiabatic flux at the outer boundary scales with $f_p(R_{\text{max}})$, which is small (see §5 for more discussion), whereas the diffusive flux is independent of $f_p(R_{\text{max}})$. The flat CR density profile simply decreases in normalization with time (Fig 5e). Similar to Perseus, Coma’s gamma-ray flux declines quickly with time, particularly at the high energies associated with imaging air Cherenkov telescopes.

Spectral steepening in Coma’s radio emission has been seen in multi-frequency observations (Brunetti et al. 2012), a feature which occurs naturally in our models due to the energy dependence of CR streaming. We show this in Fig 6; spectral steepening very similar to that observed arises. Given the flat inferred profile of Coma, which suggests that substantial streaming has already taken place, this raises

the possibility that a power-law population with a slightly higher normalization was transformed by streaming into the curved population we see today.

We have chosen a rather extreme case of a completely flat profile, to illustrate that radio halo turn-off is still possible in this case. The observational data also permit an initial CR profile that is less flat. Using the same B-field, we can still reproduce the observations very well with a profile that has a mild central peak. Since we now have a significant density gradient, the radio luminosity can drop off faster in the beginning, although the overall evolution is qualitatively the same as before. The streaming speeds ramp up faster than in the flat profile fit.

We have assumed a magnetic field profile $B \propto \rho^{\alpha_B}$, with $\alpha_B = 0.3$. This choice assumes the B-field is in rough equipartition with turbulence, as discussed in §2.4, agrees with Faraday rotation measures, and enables us to reproduce the observed surface brightness distribution. However, the Faraday rotation measurements are consistent with a range of values $\alpha_B \sim 0.4 - 0.7$ at 1σ (Bonafede et al. 2010). A steeper scaling of B with density implies lower B-fields at the cluster outskirts; in this case the rate of turn-off and development of spectral steepening will be slower. While lowering B decreases the Alfvén speed, the dominant effect is a decrease in the CR flux F due to streaming, which scales as $B^{3/2}/L_{\text{MHD}}^{1/2}$ (equation (28)). The rate of CR streaming is set by the minimum value of this flux, which generally occurs at the cluster outskirts. As we shall see in §5, in this regime we can approximate $f_p \approx 3F(R_f, p)/R_f$. Specializing to our model for Coma ($4\pi p^3 f_p(t=0) \approx 10^{-13} \text{ cm}^{-3}$ for $p = 100$, $n_e(0)/n_e(1 \text{ Mpc}) \approx 17$, and $B_0 = 5 \mu\text{G}$):

$$t_{\text{off}} \sim \left. \frac{f_p}{\dot{f}_p} \right|_{1 \text{ Mpc}} \sim 370 \text{ Myr} L_{\text{MHD},100}^{1/2} 70^{\alpha_B - 0.5} \quad (77)$$

Thus, a steeper scaling $\alpha_B = 0.7$ would not permit turn off on an acceptably short timescale for a very flat profile (it could still be possible for a less flat profile, as above, but note that the observations cannot be fit well by a centrally peaked CR profile with this steep B-field scaling). Note that radio relic measurements are consistent with strong, $\sim \mu\text{G}$ fields at the cluster outskirts (Feretti et al. 2012); in addition, the very strong turbulence at the cluster outskirts could be consistent with lower values of L_{MHD} than the constant value we have assumed. As we reiterate in the Conclusions, complex issues regarding magnetic field topology and strength are best further explored with 3D MHD simulations.

5 ANALYTIC EXPRESSIONS

In certain limiting cases, the evolution of the CR population can be derived analytically. These solutions serve two purposes: they serve as tests of our numerical code, particularly the regularization scheme (§3.1), and they also give physical insight into the behaviour of our solutions, and the circumstances under which particular processes dominate.

In the absence of sources Q and ignoring the negligible Coulomb and hadronic losses, we can write the CR transport equation (38) as:

$$\frac{Df_p}{Dt} \approx \frac{\partial f_p}{\partial t} \approx -\nabla \cdot \mathbf{F} \quad (78)$$

where the total CR flux $\mathbf{F} = \mathbf{F}_{\text{adia}} + \mathbf{F}_{\text{str}} + \mathbf{F}_{\text{turb}}$, is made

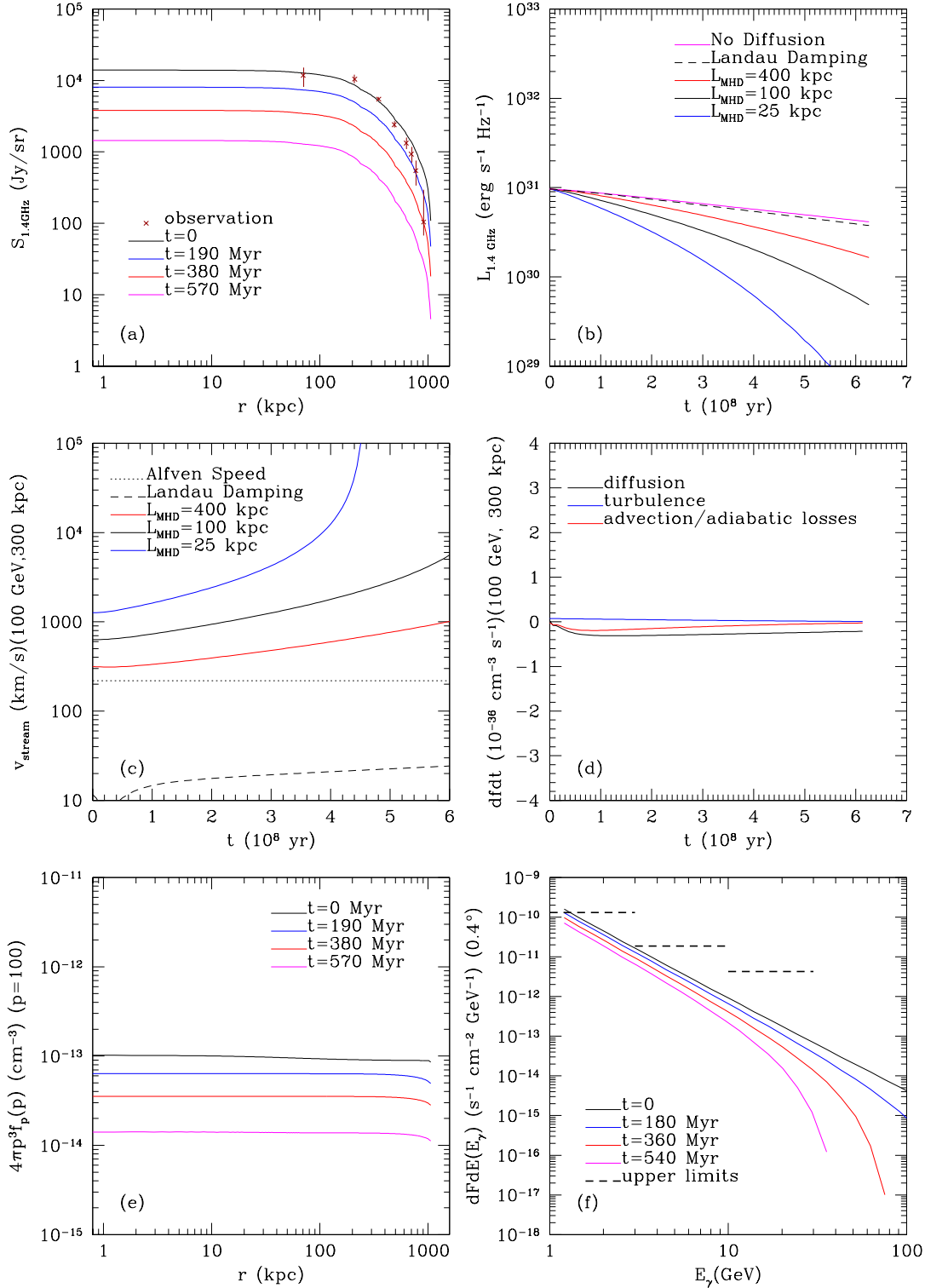


Figure 5. Simulation results for the Coma cluster. (a) Radio surface brightness of Coma for $L_{\text{MHD}} = 100$ kpc. Observations from Deiss et al. (1997). (b) The time evolution of the Coma cluster’s radio luminosity for different levels of damping. The solid lines show MHD turbulence damping at various strengths. The dashed line shows non-linear Landau damping. (c) Cosmic ray streaming speeds of 100 GeV CRs at a fixed radius of 300 kpc. (d) Different contributions to \dot{f}_p for the $L_{\text{MHD}} = 100$ kpc simulation. (e) Radial distribution of 100 GeV protons for $L_{\text{MHD}} = 100$ kpc. (f) Predicted gamma-ray fluxes. Upper limits are taken from (Arlen et al. 2012) with $\alpha = 2.5$.

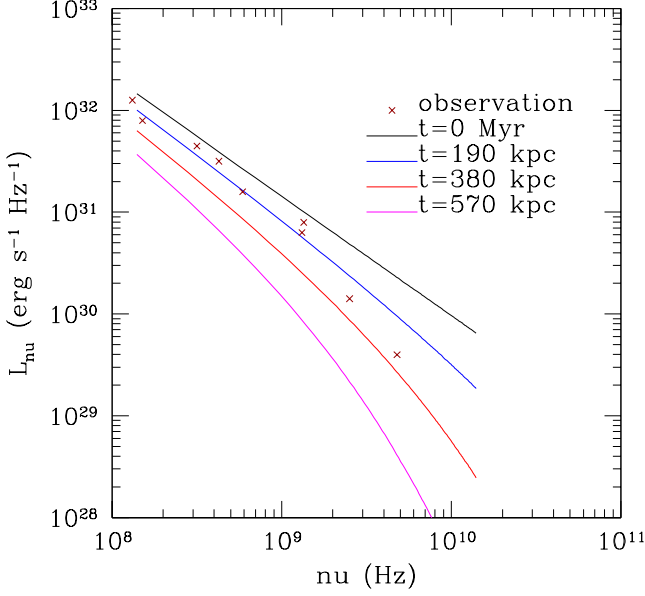


Figure 6. Luminosity as a function of energy for the Coma simulation including observations from (Brunetti et al. 2012). The momentum dependence of the streaming speed leads to a spectral steepening very similar to observation.

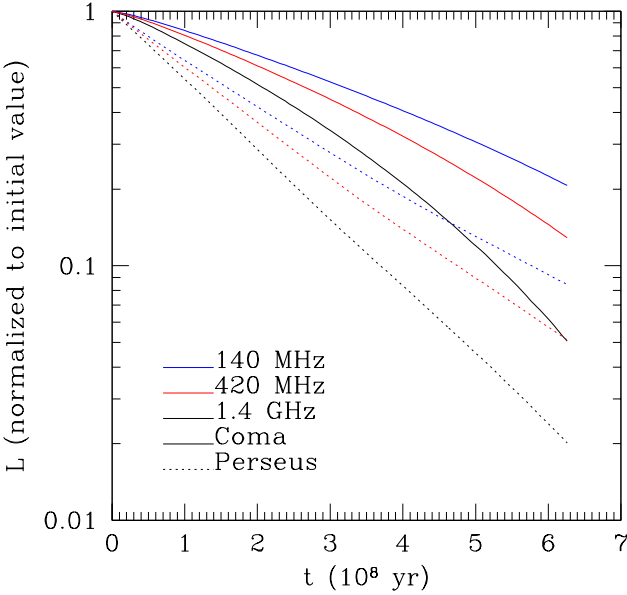


Figure 7. Luminosity dropoff in Coma for different frequencies. High energy CRs stream more quickly, so the higher frequency signals drop faster.

up of the fluxes due to adiabatic losses in the wave frame, streaming relative to the wave frame, and turbulent advection respectively. We have approximated the Lagrangian derivative by the Eulerian derivative $Df_p/Dt \approx \partial f_p/\partial t$, since $\mathbf{v}_A \cdot \nabla f_p$ is initially small and becomes increasingly negligible as the profile flattens.

As we have seen, the CR profile generally develops a flat inner core within some radius R_f , outside of which it declines. The flat core stems from the fact that while $\nabla \cdot \mathbf{F}$

increases inward¹⁰, an inverted CR profile cannot develop, since CRs cannot stream up a gradient. Thus, a flat core develops, while its normalization and radius R_f evolves due to the net flux of CRs from its outer boundary. In particular, if we set $\mathbf{F} = F\hat{\mathbf{r}}$ and integrate equation (78) over the volume of the flat region, we obtain:

$$\frac{4}{3}\pi R_f^3 \dot{f}_p(R_f, p) = -4\pi R_f^2 F(R_f, p)$$

$$\dot{f}_p(R_f, p) = -\frac{3F(R_f, p)}{R_f} \quad (79)$$

where we have used the fact that $\dot{f}_p(r, p, t)$ is independent of r for $r < R_f$, and the divergence theorem. The evolution of the entire profile can then be described by

$$\dot{f}_p(r, p, t) = \begin{cases} -\frac{3F(R_f(p, t), p, t)}{R_f(p, t)}, & r < R_f(p, t) \\ -\nabla \cdot \mathbf{F}(r, p, t), & r > R_f(p, t) \end{cases} \quad (80)$$

where the ‘‘flatness front’’ $R_f(p, t)$ is determined from $f_p(0, p, t) = f_p(R_f(p, t), p, t)$, or:

$$f_p(0, p, 0) - \int_0^t \frac{3F(R_f(p, t'), p, t')}{R_f(p, t')} dt' = f_p(R_f(p, t), p, 0) - \int_0^t \nabla \cdot \mathbf{F}(R_f(p, t'), p, t') dt' \quad (81)$$

As we have seen, $\mathbf{F}_{\text{stream}}$ and \mathbf{F}_{adia} are the most important fluxes, while \mathbf{F}_{turb} is subdominant. Let us now consider the limiting cases when only one is at play.

Cosmic-Ray streaming only. We have:

$$\mathbf{F}_{\text{stream}} = \frac{\Gamma_D B^2 \hat{\mathbf{r}}}{4\pi^3 p^3 m \Omega_0 v_A} = F_{\text{stream}} \hat{\mathbf{r}} \quad (82)$$

Since F_{stream} is independent of f_p and depends only on plasma parameters (specifically, the B-field, turbulence and density profiles), in our model where the gas properties are time-steady (and thus in hydrostatic and thermal equilibrium), $F_{\text{stream}}(r, p)$ is independent of time. Thus, $A(r, p) \equiv \nabla \cdot \mathbf{F}_{\text{stream}}(r, p)$ is also time-independent, and we have for $r > R_f(p, t)$:

$$f(r, p, t) = f(r, p, 0) - A(r, p)t; \quad r \geq R_f(p, t) \quad (83)$$

i.e., the distribution function outside the flatness front falls linearly with time. More generally, we can solve for the flatness front R_f and the overall solution both inside and outside R_f via equations (80) and (81).

To compare this analytic solution with our simulation we ran a simulation for Perseus and for Coma where only the diffusion term was used in (38), and all other terms ignored. The resulting CR densities for Perseus can be seen in figure 8. In this plot we show the CR density versus time at 100 GeV at a few select radii. The solid curves are the simulation, and the dotted lines are the analytic solution for a non-flat profile. The match is essentially perfect - the densities decrease at a constant rate (equation (83)) until the flatness front catches up to each radius. After this point the densities follow the same single curve corresponding to the

¹⁰ This condition holds as long as \mathbf{F} increases more slowly than r . In our case, the dominant fluxes $F_{\text{stream}} \propto B^{3/2} \propto \rho^{3\alpha_B/2}$ (equation (82)) clearly increases inward, and $F_{\text{adia}} \propto f v_A$ is at most flat or increases inward. Thus, $|\nabla \cdot \mathbf{F}|$ clearly increases inward.

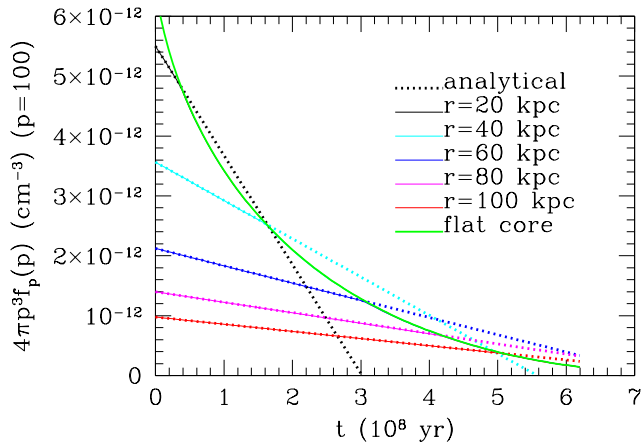


Figure 8. CR densities at 100 GeV for Perseus if only the flux from CR streaming $\mathbf{F}_{\text{stream}}$ (equation (82)) is important. The dotted lines (bold curve) show the analytic solution for outside (inside) the flat front respectively; the solution initially follows the dotted curves until it intersects the green curve, when it follows the flat front solution. The solid lines show the simulation results, which match the analytic solution almost perfectly.

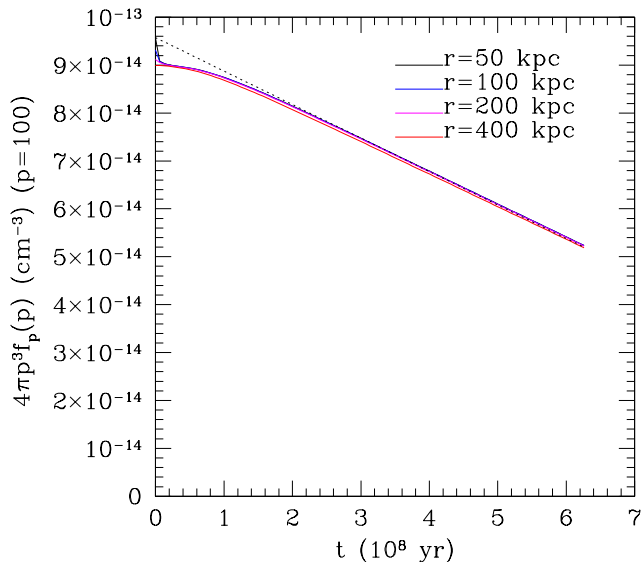


Figure 9. The same as for Fig 8 but for Coma. Since the profile is already almost flat, this is a test of the $\dot{f}_p = -3F_{\text{cr}}(R_f)/R_f = \text{constant}$ regime.

evolution of the flat region. The same results for Coma show the agreement in the regime when the profile is already flat. In figure 9, the CR profile in Coma is nearly flat to begin with. Before very long the profile is flat across the entire simulated space and the $\dot{f}_p = -3F_{\text{cr}}(R_f)/R_f$ regime kicks in. Again, the agreement between simulation and analytic solution is very good. This implies that our regularization of the CR streaming term (which is needed to prevent unphysical oscillations with such flat profiles) is not so strong that it artificially changes the rate of diffusion.

Adiabatic expansion only. We have:

$$\mathbf{F}_{\text{adia}} = \frac{1}{3}p \frac{\partial f_p}{\partial p} \mathbf{v}_A \quad (84)$$

Thus, unlike the preceding case, the flux depends on the dis-

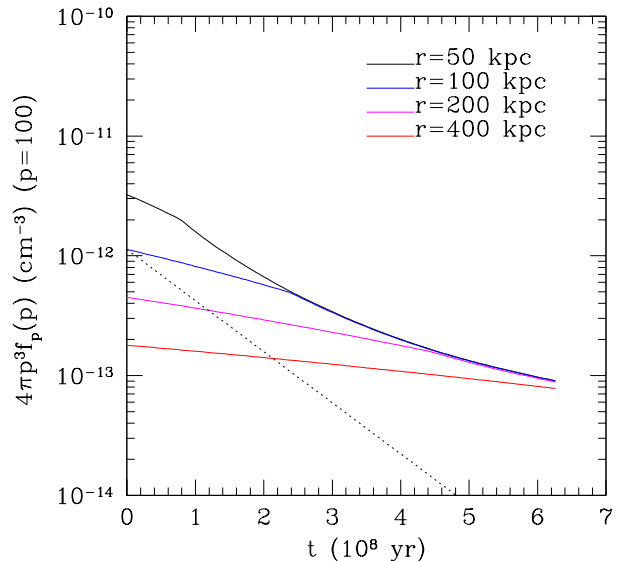


Figure 10. CR densities for Perseus in the absence of any diffusion, i.e. only adiabatic losses are used. The dotted line represents the analytic solution (85) and should be compared to the blue line.

tribution function f_p and hence is time-dependent. We can readily solve this in the approximation that $v_A \propto \rho^{\alpha_B - 0.5} \sim \text{const}$ (since it varies very weakly with radius), and $f_p \propto p^{-\alpha}$, approximately independent of radius. Then, for $r \geq R_f$, we have $\dot{f} = \nabla \cdot \mathbf{F}_{\text{adia}} \approx -2\alpha v_A f_p / 3r$, or:

$$f_p(r, p, t) \approx f_p(r, p, 0) \exp\left(-\frac{2\alpha v_A t}{3r}\right); \quad r \geq R_f \quad (85)$$

Thus, outside the flatness front, the distribution function falls exponentially with time, with e-folding time of order the Alfvén crossing time (which becomes long at large radii). To solve for the evolution of the flatness front and the entire profile, we insert equation (85) into equation (84) and hence equation (80) and (81). Note that we are only required to evaluate the flux \mathbf{F}_{adia} for $r \geq R_f$, where equation (85) is valid. We compare this analytic expression with a Perseus simulation that has no diffusion in Fig 10. The dashed line depicts (85) for $r = 100$ kpc and $p = 100$. Although the fit isn't perfect, the simulated values do fall exponentially with time until the flatness front catches up, with e-folding time comparable to that determined from (85). This is perhaps to be expected, since (85) assumes that the quantity αf_p does not vary significantly with radius, which is not typically the case.

These solutions allow us to understand the nature of the numerical solutions we previously obtained. Coma, where the initial profile is almost completely flat, is obviously in the $\dot{f}_p = -3F(R_{\text{max}})/R_f$ regime; moreover, $\mathbf{F}_{\text{stream}}(R_f) \gg \mathbf{F}_{\text{adia}}(R_f)$, since the latter scales with the (small) value of the distribution function at the outer boundary. The evolution of the flatness front in Perseus is more interesting. Initially, even though $v_D - v_A \sim \mathcal{O}(v_A)$, adiabatic losses dominate, since the distribution function falls exponentially with time (rather than linearly with time, for streaming losses). However, $\mathbf{F}_{\text{adia}} \propto f$ also falls exponentially with time, while $\mathbf{F}_{\text{stream}}$ is independent of time. Thus, streaming losses will always dominate at late times. Equivalently, the velocity associated with adiabatic losses, v_A , is constant with time,

while the streaming velocity $v_D \propto 1/f_p$ increases with time: as the number density of cosmic rays fall, the confining wave amplitude $\delta B/B$ falls, and cosmic rays can stream progressively faster.

6 CONCLUSIONS

Shocks generated during hierarchical structure formation are expected to accelerate cosmic rays via diffusive shock acceleration. These cosmic rays in turn interact hadronically with thermal nucleons to produce pions, which decay to produce relativistic electrons. Tracking these well-understood processes, and assuming magnetic fields given by Faraday rotation measurements, leads to predictions for radio halo emission consistent with those observed (Pfrommer 2008). However, this model predicts that *every* cluster hosts a bright radio halo. This is at odds with the observed bimodality of cluster radio emission: the majority of clusters are radio-quiet, and an order of magnitude fainter than the radio-loud population (Feretti et al. 2012; Brown et al. 2011). Radio loudness is strongly associated with merger activity. For this reason, the turbulent re-acceleration model (Brunetti et al. 2001; Petrosian 2001), where this association occurs naturally, is often favored. However, this still begs the question as to *why* hadronically induced radio emission is not omnipresent. All of the associated physics is well understood, and at face value the observations then require that CRp acceleration efficiencies be reduced by an order of magnitude below canonical values¹¹.

Enßlin et al. (2011) took an important step forward when they suggested that CRp's could potentially stream super-Alfvénically, turning off radio halos. However, they assumed streaming speeds of order the sound speed $v_D \sim c_s$ instead of calculating it¹², and posited steady-state CR profiles that represent equilibria between outward streaming and inward turbulent advection, despite the long timescales for equilibration. In this paper, we attempt to place CR streaming in clusters on a more rigorous footing, by calculating the microphysical streaming speed as a function of plasma parameters in the self-confinement picture (Lerche 1967; Kulsrud & Pearce 1969; Wentzel 1969; Skilling 1971). We then solve the time-dependent CR transport equation (albeit in 1D) to see how the radio luminosity evolves with time. Our conclusions are as follows:

- CR streaming speeds depend on the source of wave damping. Non-linear Landau damping (e.g., (Felice & Kulsrud 2001), as assumed in Enßlin et al. (2011)) is too weak to sufficiently inhibit wave growth, and $v_D \sim v_A$. However, if waves are instead damped by turbulent shear (Yan & Lazarian 2002; Farmer & Goldreich 2004), they can be sufficiently suppressed that super-Alfvénic streaming $v_D \gg v_A$ is possible. Moreover, $v_D - v_A \propto \gamma/n_{CR}(> \gamma)$, (where γ is the CR Lorentz factor) so that: i) higher energy cosmic rays stream

more rapidly; ii) CR streaming speeds continually increase as n_{CR} declines due to streaming.

- Streaming relative to the Alfvén wave frame can be incorporated into the CR transport equation via a diffusion term. For turbulent wave damping, the diffusion coefficient $\kappa \propto 1/\nabla f_p$ (where f_p is the distribution function), so that remarkably $\nabla \cdot (\kappa \nabla f_p)$ is *independent* of ∇f_p . Thus, CRs can continue to stream unabated in giant radio halos (such as Coma) despite their fairly flat inferred CR profiles. Streaming is still sensitive to the *sign* of ∇f_p (since CRs can only stream down a gradient), and for flat profiles we must implement numerical regularization (Sharma et al. 2009) to ensure stable solutions. We test our solver for the CR distribution function against a code where CR mediated AGN heating is solved in the fluid approximation (Guo & Oh 2008). The solutions are identical. Note that CR heating is unaffected by super-Alfvénic streaming, since it scales as $\mathbf{v}_A \cdot \nabla P_c$ and P_c is dominated by \sim GeV CRs, where streaming is Alfvénic.

- CR transport is thus clearly modified by ICM turbulence. Besides its effects on wave damping, turbulence can also advect CRs so that they roughly trace the gas density profile, creating a centrally peaked CR distribution. For the mildly subsonic $v_s \sim v_A \sim 100 \text{ km s}^{-1}$ turbulence we assume, outward streaming dominates inward advection. Moreover, this trend *increases* with the amplitude of turbulence. It is therefore consistent with the flat inferred CR profiles in non cool-core clusters, which have generally stronger turbulent motions. Such a trend is hard to understand in scenarios where turbulence only draws CRs inward (Enßlin et al. 2011; Zandanel, Pfrommer & Prada 2012).

- We then perform numerical time-dependent calculations of CR streaming, assuming an initial profile consistent with radio observations at 1.4 GHz. We find that the radio luminosity falls by an order of magnitude in several hundred Myr, both in a prototypical radio mini-halo (Perseus) and giant radio halo (Coma). The latter effect is particularly interesting in light of the flat inferred CR profile, and arises *only* for turbulent damping of MHD waves; if only non-linear Landau damping is at play, the turn-off is slow. Indeed, the inferred flatness of the CR profile suggests that streaming has already been at play in these systems. We also build an analytic model which aids in physical understanding. Adiabatic losses dominate until the profile flattens, when diffusive losses dominate. The turn-off timescale in the later stage is set by the lowest value of the CR flux $F \propto B^{3/2}/L_{\text{MHD}}$, generally at the cluster outskirts. The energy-dependence of CR streaming means that spectral curvature develops, and radio halos turn off more slowly at low frequencies, both consistent with observations (Brunetti et al. 2008, 2012). Streaming also rapidly diminishes the γ -ray luminosities at the $E_\gamma \sim 0.3 - 1 \text{ TeV}$ energies probed by imaging air Cerenkov telescopes (MAGIC, HESS, VERITAS), but not for the lower energies $E_\gamma \sim 0.1 - 3 \text{ GeV}$ probed by Fermi. The latter is therefore a more robust probe of the CR injection history.

The primary contribution of this paper is a physical proof of principle for turning off hadronically induced emission. Our 1D streaming calculations by nature omit important details best clarified by 3D MHD simulations. Chief amongst these are the effects of magnetic topology. We have effectively assumed radial magnetic fields in our 1D calcu-

¹¹ A bimodality in cluster B-fields, with larger values during the turbulent, radio-loud state, appears inconsistent with cluster rotation-measure observations (Bonafede et al. (2011), and references therein).

¹² In fact, given their assumptions, we find that cosmic rays should only stream Alfvénically.

lations. Of course, magnetic topology greatly influences the true value of macroscopic transport coefficients. There is some evidence both from observations (Pfrommer & Dursi 2010) and cosmological MHD simulations (Ruszkowski et al. 2011) that outside the core, magnetic fields are largely radial, driven either by cosmological infall, or the magneto-thermal instability (MTI; Balbus (2000); Parrish, Stone & Lemaster (2008)). Alternatively, turbulence could fully tangle magnetic fields (Ruszkowski & Oh 2010, 2011; Parrish, Quataert & Sharma 2009). CRs have to follow the same field lines that thermal particles do, albeit with a larger gyro radius¹³. As long as cross-field diffusivity remains small, transport coefficients should scale similarly; in the limit of a fully tangled field with a coherence length significantly larger than the gyro radius, a random walk in 3D rather than 1D will reduce the diffusion coefficient $\kappa_p \rightarrow \kappa_p/3$, just as it reduces the Spitzer-Braginskii value for thermal conductivity by a factor of 3. This will effectively increase all quoted timescales in this paper for pure streaming by a factor of ~ 3 . In the future, it would be interesting to conduct fully self-consistent 3D MHD simulations which include CR streaming, motivated and guided by the estimates here. We have also incorporated the advective effects of gas motions only in the diffusive approximation. Coherent bulk motions due to mergers or sloshing could potentially have stronger effects. More light on the nature of ICM motions in radio-bright halos from Astro-H (e.g., Zhuravleva et al. (2012); Shang & Oh (2012b,a)) will surely help. We are also agnostic as to the cause of radio halo turn-on, which is clearly related to gas motions stimulated by mergers, and could be due to turbulent reacceleration of seed CRs (Brunetti et al. 2001; Petrosian 2001), inward advection of CRs from the cluster outskirts (Enßlin et al. 2011), or perhaps have separate mechanisms for different classes of radio halos (Zandanel, Pfrommer & Prada 2012). Such issues await clarification from low frequency radio observations by LOFAR.

ACKNOWLEDGMENTS

We acknowledge NSF grant 0908480 and NASA grant NNX12AG73G for support. We are grateful to Christoph Pfrommer for sparking our interest in this topic and stimulating discussions. We also thank Gianfranco Brunetti, Torsten Ensslin, Anders Pinzke and Ellen Zweibel for helpful conversations. SPO also thanks the KITP (supported by NSF PHY05-51164), the Aspen Center for Physics (NSF Grant No. 1066293) and UCLA for hospitality, and the Getty Center for inspiring views, during the completion of this paper.

REFERENCES

Achterberg A., 1981, *A&A*, 98, 161
 Aleksić J. et al., 2012, *A&A*, 541, A99
 Arlen T. et al., 2012, *ApJ*, 757, 123

¹³ Interestingly, 100 GeV CRs have a mean free path due to wave-particle interactions $\lambda_{\text{CR}} \sim (\delta B/B)^{-2} r_L \sim 1 - 10 \text{ kpc} B_{\mu\text{G}}^{-1} \epsilon_{100 \text{ GeV}} ([\delta B/B]/10^{-4})^{-2}$ which is similar to the electron collisional mean free path $\lambda_e \sim 6 \text{ kpc} T_{4 \text{ keV}}^2 n_{i,-3}$.

Balbus S. A., 2000, *ApJ*, 534, 420
 Battaglia N., Bond J. R., Pfrommer C., Sievers J. L., 2012, *ApJ*, 758, 74
 Bell A. R., 1978, *MNRAS*, 182, 443
 Berezhinsky V. S., Blasi P., Ptuskin V. S., 1997, *ApJ*, 487, 529
 Blandford R., Eichler D., 1987, *Phys. Rep.*, 154, 1
 Boehringer H., Morfill G. E., 1988, *ApJ*, 330, 609
 Bonafede A., Feretti L., Murgia M., Govoni F., Giovannini G., Dallacasa D., Dolag K., Taylor G. B., 2010, *A&A*, 513, A30
 Bonafede A., Govoni F., Feretti L., Murgia M., Giovannini G., Brüggem M., 2011, *A&A*, 530, A24
 Briel U. G., Henry J. P., Boehringer H., 1992, *A&A*, 259, L31
 Brown S., Emerick A., Rudnick L., Brunetti G., 2011, *ApJ*, 740, L28
 Brown S., Rudnick L., 2011, *MNRAS*, 412, 2
 Brunetti G., Blasi P., Reimer O., Rudnick L., Bonafede A., Brown S., 2012, *MNRAS*, 426, 956
 Brunetti G. et al., 2008, *Nat*, 455, 944
 Brunetti G., Lazarian A., 2007, *MNRAS*, 378, 245
 Brunetti G., Setti G., Feretti L., Giovannini G., 2001, *MNRAS*, 320, 365
 Capelo P. R., Coppi P. S., Natarajan P., 2012, *MNRAS*, 422, 686
 Chandran B. D. G., 2000, *Physical Review Letters*, 85, 4656
 Chandran B. D. G., Rasera Y., 2007, *ApJ*, 671, 1413
 Chen C. H. K., Mallet A., Yousef T. A., Schekochihin A. A., Horbury T. S., 2011, *MNRAS*, 415, 3219
 Cho J., Vishniac E. T., 2000, *ApJ*, 539, 273
 Churazov E., Forman W., Jones C., Böhringer H., 2003, *ApJ*, 590, 225
 Deiss B. M., Reich W., Lesch H., Wielebinski R., 1997, *A&A*, 321, 55
 Dubois Y., Teyssier R., 2008, *A&A*, 482, L13
 Enßlin T., Pfrommer C., Miniati F., Subramanian K., 2011, *A&A*, 527, A99+
 Enßlin T. A., Biermann P. L., Kronberg P. P., Wu X.-P., 1997, *ApJ*, 477, 560
 Enßlin T. A., Pfrommer C., Springel V., Jubelgas M., 2007, *A&A*, 473, 41
 Ensslin T. A., Wang Y., Nath B. B., Biermann P. L., 1998, *A&A*, 333, L47
 Farmer A. J., Goldreich P., 2004, *ApJ*, 604, 671
 Felice G. M., Kulsrud R. M., 2001, *ApJ*, 553, 198
 Feretti L., Giovannini G., Govoni F., Murgia M., 2012, *AAPR*, 20, 54
 Ferland G. J., Fabian A. C., Hatch N. A., Johnstone R. M., Porter R. L., van Hoof P. A. M., Williams R. J. R., 2008, *MNRAS*, 386, L72
 —, 2009, *MNRAS*, 392, 1475
 Foote E. A., Kulsrud R. M., 1979, *ApJ*, 233, 302
 Goldreich P., Sridhar S., 1995, *ApJ*, 438, 763
 Guo F., Oh S. P., 2008, *MNRAS*, 384, 251
 Holman G. D., Ionson J. A., Scott J. S., 1979, *ApJ*, 228, 576
 Horbury T. S., Forman M., Oughton S., 2008, *Physical Review Letters*, 101, 175005
 Kuchar P., Enßlin T. A., 2011, *A&A*, 529, A13
 Kulsrud R., Pearce W. P., 1969, *ApJ*, 156, 445

- Kulsrud R. M., 1978, in *Astronomical Papers Dedicated to Bengt Stromgren*, Reiz A., Andersen T., eds., pp. 317–326
- , 2005, *Plasma physics for astrophysics*. Princeton University Press
- Kulsrud R. M., Cesarsky C. J., 1971, *Astrophys. Lett.*, 8, 189
- Kunz M. W., Schekochihin A. A., Cowley S. C., Binney J. J., Sanders J. S., 2011, *MNRAS*, 410, 2446
- Lee M. A., Völk H. J., 1973, *Astrophysics and Space Science*, 24, 31
- Lerche I., 1967, *ApJ*, 147, 689
- Lithwick Y., Goldreich P., 2001, *ApJ*, 562, 279
- Loewenstein M., Zweibel E. G., Begelman M. C., 1991, *ApJ*, 377, 392
- Loken C., Norman M. L., Nelson E., Burns J., Bryan G. L., Motl P., 2002, *ApJ*, 579, 571
- Mannheim K., Schlickeiser R., 1994, *A&A*, 286, 983
- Maron J., Goldreich P., 2001, *ApJ*, 554, 1175
- McNamara B. R., Nulsen P. E. J., 2007, *ARA&A*, 45, 117
- Miller J. A., 1991, *ApJ*, 376, 342
- Miniati F., Ryu D., Kang H., Jones T. W., 2001, *ApJ*, 559, 59
- Nachtmann O., 1990, *Elementary particle physics: Concepts and phenomena*. Springer
- Nazarenko S. V., Schekochihin A. A., 2011, *Journal of Fluid Mechanics*, 677, 134
- Parrish I. J., Quataert E., Sharma P., 2009, *ApJ*, 703, 96
- Parrish I. J., Stone J. M., Lemaster N., 2008, *ApJ*, 688, 905
- Pedlar A., Ghataure H. S., Davies R. D., Harrison B. A., Perley R., Crane P. C., Unger S. W., 1990, *MNRAS*, 246, 477
- Petrosian V., 2001, *ApJ*, 557, 560
- Pfrommer C., 2008, *MNRAS*, 385, 1242
- Pfrommer C., Dursi J., 2010, *Nature Physics*, 6, 520
- Pfrommer C., Enßlin T. A., 2004, *A&A*, 413, 17
- Pfrommer C., Enßlin T. A., Springel V., 2008, *MNRAS*, 385, 1211
- Pinzke A., Pfrommer C., 2010, *MNRAS*, 409, 449
- Podesta J. J., 2009, *ApJ*, 698, 986
- Rebusco P., Churazov E., Böhringer H., Forman W., 2006, *MNRAS*, 372, 1840
- Ruszkowski M., Lee D., Brügggen M., Parrish I., Oh S. P., 2011, *ApJ*, 740, 81
- Ruszkowski M., Oh S. P., 2010, *ApJ*, 713, 1332
- , 2011, *MNRAS*, 414, 1493
- Rybicki G. B., Lightman A. P., 1979, *Radiative Processes in Astrophysics*. New York: Wiley
- Schlickeiser R., 2002, *Cosmic Ray Astrophysics*. Berlin: Springer
- Shang C., Oh S. P., 2012a, *ArXiv e-prints*
- , 2012b, *MNRAS*, 426, 3435
- Sharma P., Chandran B. D. G., Quataert E., Parrish I. J., 2009, *ApJ*, 699, 348
- Sharma P., Colella P., Martin D. F., 2010, *SIAM J. of Scient. Comp.*, 32, 3564
- Shaw L. D., Nagai D., Bhattacharya S., Lau E. T., 2010, *ApJ*, 725, 1452
- Skilling J., 1971, *ApJ*, 170, 265
- Uhlig M., Pfrommer C., Sharma M., Nath B. B., Enßlin T. A., Springel V., 2012, *MNRAS*, 423, 2374
- Völk H. J., Aharonian F. A., Breitschwerdt D., 1996, *Space Science Reviews*, 75, 279
- Wentzel D. G., 1969, *ApJ*, 156, 303
- Wicks R. T., Horbury T. S., Chen C. H. K., Schekochihin A. A., 2010, *MNRAS*, 407, L31
- Yan H., Lazarian A., 2002, *Physical Review Letters*, 89, B1102+
- , 2004, *ApJ*, 614, 757
- , 2008, *ApJ*, 673, 942
- Zandanel F., Pfrommer C., Prada F., 2012, *ArXiv e-prints*
- Zhuravleva I., Churazov E., Kravtsov A., Sunyaev R., 2012, *ArXiv e-prints*